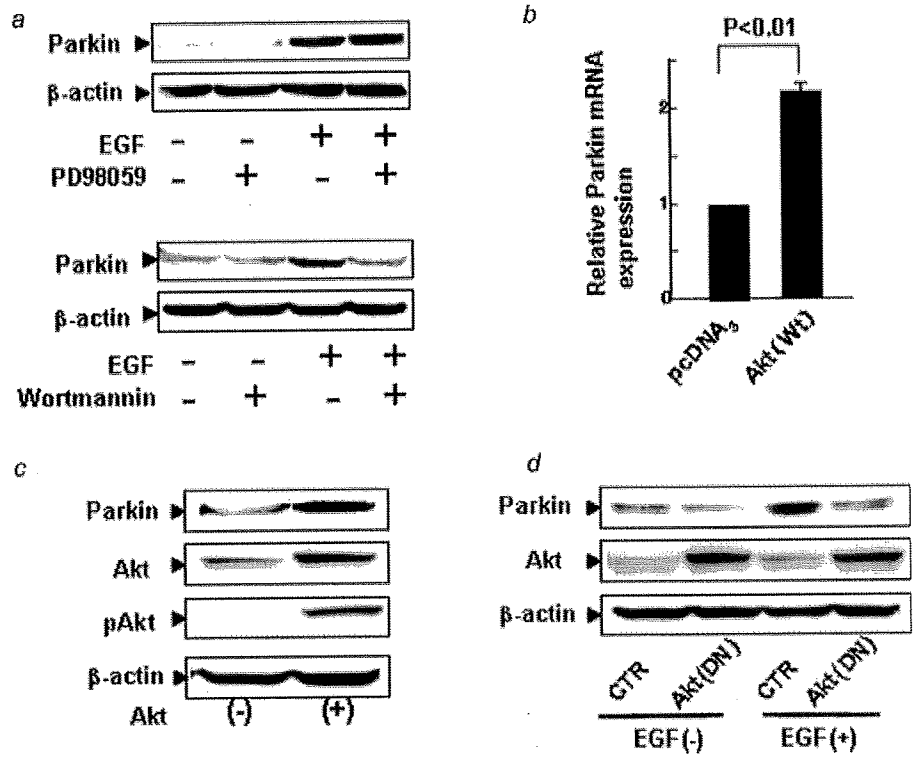

FIGURE 3 – EGF-mediated Parkin expression is induced via the Akt-signaling pathway. (*a*) Effects of the MEK-inhibitor PD98059 or Akt-inhibitor wortmannin on EGF-mediated Parkin expression. HT29 cells were treated with PD98059 (10 μM) or wortmannin (1 μM) for 30 min, and further subjected to EGF (100 ng/ml) stimulation for 18 hr. Cell lysates were probed with anti-Parkin (upper panel) or anti-β-actin (lower panel) antibodies. (*b,c*) HT29 cells were transfected with plasmid for the expression of wild-type human Akt [Akt(+)] or with a control vector [Akt(−)]. After 18 hr, lysates of the transfected cells were subjected to quantitative RT-PCR analyses (*b*) or immunoblotting (*c*) with anti-Parkin (upper panel), anti-Akt (Akt; upper middle panel), anti-phospho Akt (lower middle panel), or anti-β-actin (lower panel) antibodies. (*d*) Expression plasmids encoding a dominant-negative form of human *Akt* (DN) or a control vector (CTR) were transfected into HT29 cells and then treated with EGF (100 ng/ml) for 18 hr. Each sample was harvested and the extracted cell lysates were probed with anti-Parkin (upper panel), anti-Akt (Akt; middle panel) or anti-β-actin (lower panel) antibodies.

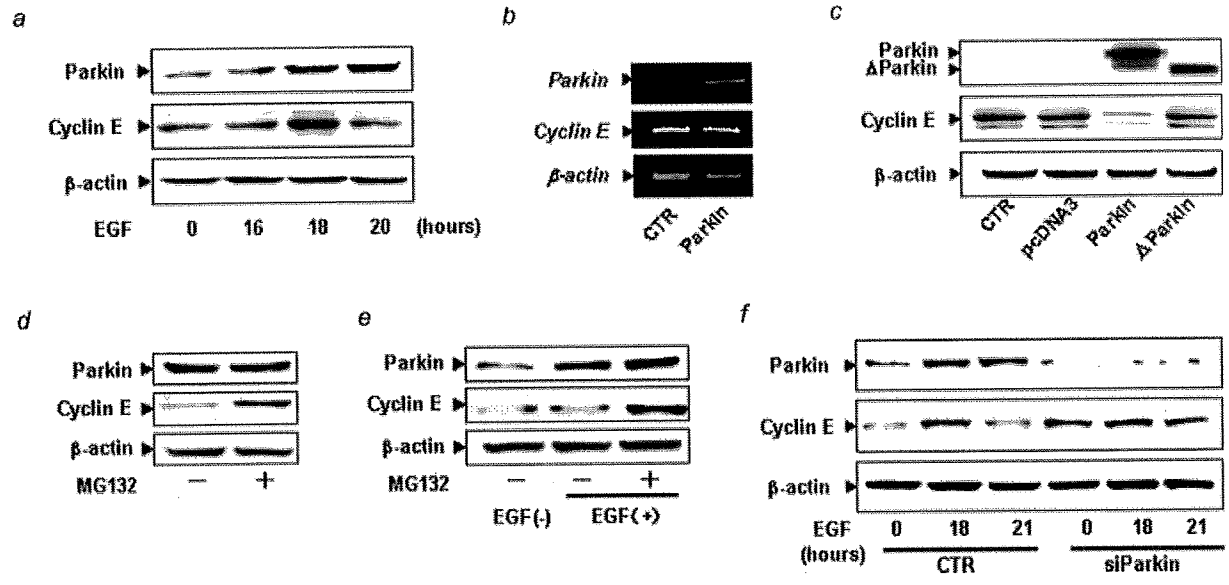

FIGURE 4

assessed the time-course changes of the cyclin E protein expression in the colon cells. Knockdown of endogenous *Parkin* by siRNA resulted in the consistent upregulation of cyclin E protein after the treatment with EGF (Fig. 4*f*). These findings suggest that Parkin contributes to the proteolytic degradation of cyclin E protein in human colon cells..

Alternative splicing isoforms of Parkin with loss of cyclin E proteolysis were dominantly expressed in human colorectal cancers

The findings that EGF stimulation induced Parkin expression followed by the degradation of cyclin E protein suggested that Parkin exerts negative feedback regulation of proliferation signaling in epithelial cells. To clarify the functional significance of the *Parkin* defect in tumorigenesis, we investigated the expression profiles of *Parkin* in clinical specimens of human colorectal cancer tissues. To amplify the *Parkin* transcript, we designed a primer set spanning all of the exons of the *Parkin* gene. First, we confirmed that the signal amplified by this primer set corresponded to the expected size in normal colonic tissues. In contrast, 18 of 43 (42%) human colorectal cancers predominantly expressed *Parkin* transcripts that were smaller than expected (Fig. 5*a*). To determine the internal structure of these products, all amplified fragments were subcloned for further sequence analyses. All signals with a smaller sequence size corresponded to the *Parkin* transcript with the deletion of several exons spanning from exon 3 to exon 6 (Fig. 5*b*), indicating that aberrant and alternative splicing of the *Parkin* gene occurs in human colorectal cancers. In support of the results obtained from the analyses on human clinical specimens, we found predominant expression of alternatively spliced *Parkin* in DLD1 colon cancer cells *in vitro* (Supplemental Fig. 2). DLD1 cells expressed a *Parkin* transcript lacking exons 3 to 5 and exons 7 and 8, while HT29 colon cancer cells expressed wild-type *Parkin* predominantly. Immunoblotting confirmed the expression of the alternatively spliced *Parkin* in the lysate of DLD1 cells.

To determine whether the tumor-specific isoforms of alternatively spliced *Parkin* are involved in cell cycle deregulation, we examined whether splicing variants of *Parkin* expressed in human colorectal cancer tissues were capable of inducing the proteolytic degradation of the cyclin E protein *in vitro*. We subcloned representative alternative splicing isoforms of *Parkin* from colorectal cancer tissues and constructed expression plasmids encoding the tumor-specific *Parkin* variants, including those lacking exons 3–4,

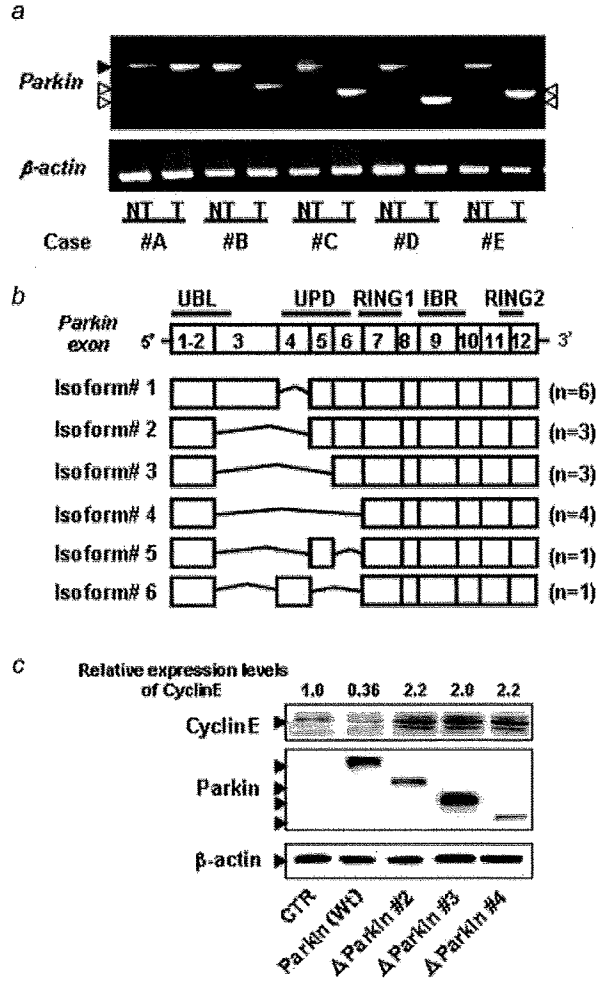

FIGURE 4 – Parkin expression triggers proteolysis of cyclin E protein in colon cells. (*a*) Time-course changes of the Parkin and cyclin E protein expression after EGF stimulation. HT29 cells were treated with EGF (100 ng/ml) at the indicated time points. Cell lysate was extracted and subjected to immunoblotting using anti-Parkin (upper panel), anti-cyclin E (middle panel) or anti-β-actin (lower panel) antibodies. Quantification of the results of Western blotting was carried out by scanning densitometry analysis using the LAS-3000 imaging system. (*b,c*) 293T cells were transfected with the expression plasmids encoding wild-type human *Parkin*, mutant *Parkin* lacking exon 3-4 (Δ-Parkin) or control vectors. (*b*) Total RNA extracted from the cells transfected with control vector (CTR) or wild-type *Parkin* expression plasmid was subjected to semiquantitative RT-PCR analyses using primers specific for *Parkin* (upper panel), cyclin E (middle panel) or β-actin (lower panel). (*c*) Lysates were also prepared from the transfected cells and immunoblotting was performed using anti-Parkin (upper panel), anti-cyclin E (middle panel) or anti-β-actin (lower panel) antibodies. (*d*) HT29 cells were treated with a proteasome inhibitor MG132 (10 μM) for 1 hr, followed by the transfection with expression plasmid encoding the wild-type*Parkin*. Immunoblotting was performed using anti-Parkin (upper panel), anti-cyclin E (middle panel) or anti-β-actin (lower panel) antibodies. (*e*) HT29 cells were treated with EGF for 22 hr in the presence or absence of MG132 (10 μM). Endogenous Parkin, cyclin E and β-actin protein expression was detected by immunoblotting analyses using anti-Parkin (upper panel), anti-cyclin E (middle panel) or anti-β-actin (lower panel) antibodies. (*f*) SW48 cells were transfected with siRNA targeting *Parkin* (siParkin) or control (CTR) siRNA for 24 hr, followed by treatment with EGF (100 ng/ml) for the additional indicated times. The cell lysates were subjected to immunoblot analyses to determine the protein production levels of anti-Parkin (upper panel), anti-cyclin E (middle panel) or anti-β-actin (lower panel).

FIGURE 5 – Alternatively spliced isoforms of *Parkin* transcripts were expressed in human colorectal cancers. (*a*) Total RNA was extracted from tumor (T) or non-tumorous (NT) regions of the colon tissues of patients with colorectal cancers. *Parkin* transcripts were determined by RT-PCR using primer sets for the amplification of full-length *Parkin* mRNA. Representative results of the gel electrophoresis of the amplified fragments from 5 patients with colorectal cancers are shown (case #A–#E). Black arrowhead indicates the fragment size of 1500 bp, corresponding to whole *Parkin* sequences of the expected size. Shorter fragments derived from *Parkin* amplification are indicated with white arrowheads. (*b*) Schematic presentation of alternatively spliced isoforms of *Parkin* expressed in colorectal cancers. The values in the schema indicate the exon number of the human *Parkin* gene. UBL, ubiquitin-like; UPD, unique Parkin domain; RING, really interesting new gene; IBR, in-between Ring; n = number of cases. (*c*) Alternative spliced Parkin proteins lacked proteolytic activity for cyclin E protein, 293T cells were transfected with expression plasmid encoding wild-type Parkin (Wt), various alternatively spliced isoforms of *Parkin* subcloned from the colon of cancer patients or a control vector (CTR). Cell lysates were prepared and subjected to immunoblotting using anti-myc (upper panel), anti-cyclin E (middle panel) or anti-β-actin (lower panel) antibodies. Quantification of the results of Western blotting was carried out by scanning densitometry analysis.

exons 3–5 and exons 3–6. We confirmed that the induction of wild-type *Parkin* reduced endogenous cyclin E protein expression. In contrast, there were slight upregulation in the expression levels of cyclin E protein in cells expressing any of the tumor-specific splicing isoforms of *Parkin* examined (Fig. 5*c*). In addition, we found that immunoreactivity for Ki67 in cells expressing *Parkin* splicing variants was substantially stronger than in cells expressing wild-type *Parkin* (Supplemental Fig. 3). These findings indicate that the alternative splicing of the *Parkin* gene might contribute to the accumulation of cyclin E protein, leading to the deregulation of cell- cycle progression in colorectal cancers.

Discussion

Parkin is an E3 ubiquitin ligase that belongs to the RING-finger family. Cyclin E may be a putative Parkin substrate.[7] In contrast to the intensive research of Parkin in neurons, little is known about the transcriptional regulation of Parkin in human epithelial cells or the role of Parkin in cell cycle regulation. We, recently, reported that *Parkin*-deficient mice lacking exon 3 of the *Parkin* gene are susceptible to liver carcinogenesis, providing the first evidence that *Parkin* is a tumor suppressor gene.[19] Consistent with our findings, a high frequency of loss of heterozygosity or deletions spanning the *Parkin* gene has been detected in various human cancers.[9–18] In the present study, we demonstrated that Parkin expression is induced in response to growth signaling, and is involved in the proteolytic degradation of cyclin E protein in colonic epithelial cells.

EGF is implicated in the growth regulation of a variety of epithelial cells.[27] Enhanced EGF signaling is involved in the pathogenesis and progression of various human cancers.[28,29] Of note, frequent overexpression of EGF receptors is observed in human colorectal cancer cells, and therefore, EGF signaling pathways have emerged as promising targets for anticancer therapy in the treatment of colorectal cancers.[30,31] The present findings suggested that the downregulation of cyclin E protein in the late phase of EGF stimulation was attributable to the upregulation of *Parkin* in colon cells. These findings support the possibility that Parkin may be involved in a negative feedback regulation of the EGF-mediated proliferation signaling in colonic cells.

The *Parkin* gene contains 12 exons and is transcribed into a 457 amino acid protein. Functional domains within the Parkin protein include an amino-terminal ubiquitin-like (UBL) domain and the cysteine-rich unique Parkin domain (UPD) followed by 2 really interesting new gene (RING) fingers.[32] We identified various alternatively spliced isoforms of *Parkin* in human colorectal cancers. Alternative splicing of *Parkin* in colorectal cancers resulted in the loss of various exons spanning exon 3 to exon 6, the region corresponding to the UPD. Notably, these alternatively spliced isoforms were defective in their ability to induce proteolytic degradation of cyclin E protein. Interestingly, point mutations of the *Parkin* gene in autosomal recessive juvenile Parkinsonism patients were clustered in the UBL, UPD and RING-finger motifs.[32] Thus, our findings support the idea that all of the structural elements, including UPD, are essential for the functional integrity of Parkin.

Alternative splicing is a biologic event whereby identical precursor mRNA is spliced in different ways, contributing to the generation of protein diversity. Alternative splicing is a widely observed phenomenon in the developmental process under physiologic conditions.[33] Recent studies suggest that alternative splicing is crucially linked to the development of cancer.[34] Indeed, many cancer-specific isoforms of tumor-related genes produced by alternative splicing have been identified in several human tumors.[34,35] The most studied alternatively spliced gene in cancers might be *CD44*, in which inclusion of variable exons correlates with tumor development and metastasis.[36] It was shown that phosphorylation of the nuclear RNA binding protein Sam68 activated by growth signaling regulates alternative splicing of variable exon 5 of the *CD44* gene in lymphoma cells.[37] The findings of the present study indicated that various alternative splicing isoforms of the *Parkin* gene were dominantly expressed in a considerable number of human colorectal cancers. The molecular mechanisms responsible for the production of different splicing variants, however, is unclear, but cancer-specific changes in the splicing pattern have been reported in various genes without mutations in cis-acting splicing elements, suggesting that alternative splicing in tumor tissues may be due to changes in the trans-acting splicing regulators.[35]

The interaction of transiently expressed cyclins with cyclin-dependent kinases (CDK) permits cell cycle progression. Cyclin E, an activator of Cdk2, is a G_1 cyclin necessary for the transition from the G_1 to S phase of the normal cell cycle.[38] Cyclin E-CDK2 activity is regulated during the cell cycle and peaks around the time of S-phase entry.[39,40] This periodicity results from changes in cyclin E abundance, and cyclin E levels are normally tightly regulated so that peak cyclin E–Cdk2 kinase activity occurs only for a short time near the G1/S boundary.[41] Cyclin E abundance is regulated by E2F-dependent cyclin E transcription and cyclin E degradation is regulated by the ubiquitin-proteasome system. Cyclin E overexpression, however, is observed in a broad spectrum of human malignancies, including colorectal cancer, suggesting that proper regulation of cyclin E is important for the preservation of normal cellular functions.[42] Indeed, overexpression of the cyclin E protein has been linked to shortening of the G_1 phase of the cell cycle,[43] enhanced cell proliferation[44] and induction of chromosomal instability.[45,46] Our present findings revealed that human colorectal cancers expressed various *Parkin* isoforms that lack the ability to degrade cyclin E protein. We also confirmed that the expression of the alternatively spliced variants of *Parkin* identified in the tumor tissues resulted in the accumulation of cyclin E protein in the cultured colon cells.

In conclusion, the findings of the present study demonstrate that *Parkin* is transcriptionally regulated in a growth factor stimulation-dependent manner and is involved in the regulation of cyclin E expression, and suggest that alternative splicing of the *Parkin* gene contributes to enhanced colon cell proliferation, leading to the progression of colorectal cancers. Further analyses are required to clarify the mechanism of tumor-specific alternative splicing of *Parkin* and the prevalence of the *Parkin* isoforms that lack cyclin E-proteolysis activity in other types of human cancers.

Acknowledgements

The authors are grateful to Dr. H. Kubo for supplying the clinical specimens.

References

1. Shimura H, Hattori N, Kubo S, Mizuno Y, Asakawa S, Minoshima S, Shimizu N, Iwai K, Chiba T, Tanaka K, Suzuki T. Familial Parkinson disease gene product, parkin, is a ubiquitin-protein ligase. Nat Genet 2000;25:302–5.
2. Imai Y, Soda M, Takahashi R. Parkin suppresses unfolded protein stress-induced cell death through its E3 ubiquitin-protein ligase activity. J Biol Chem 2000;275:35661–4.
3. Zhang Y, Gao J, Chung KK, Huang H, Dawson VL, Dawson TM. Parkin functions as an E2-dependent ubiquitin- protein ligase and promotes the degradation of the synaptic vesicle-associated protein, CDCrel-1. Proc Natl Acad Sci USA 2000;97:13354–9.
4. Wang M, Suzuki T, Kitada T, Asakawa S, Minoshima S, Shimizu N, Tanaka K, Mizuno Y, Hattori N. Developmental changes in the expression of parkin and UbcR7, a parkin-interacting and ubiquitin-conjugating enzyme, in rat brain. J Neurochem 2001;77: 1561–8.
5. Imai Y, Takahashi R. How do Parkin mutations result in neurodegeneration? Curr Opin Neurobiol 2004;14:384–9.
6. Imai Y, Soda M, Inoue H, Hattori N, Mizuno Y, Takahashi R. An unfolded putative transmembrane polypeptide, which can lead to endoplasmic reticulum stress, is a substrate of Parkin. Cell 2001; 105:891–902.

7. Staropoli JF, Mcdermott C, Martinat C, Schulman B, Demireva E, Abeliovich A. Parkin is a component of an SCF-like ubiquitin ligase complex and protects postmitotic neurons from kainate excitotoxicity. Neuron 2003;37:735–49.
8. Farrer MJ. Genetics of Parkinson disease: paradigm shifts and future prospects. Nat Rev Genet 2006;7:306–18.
9. Saito S, Sirahama S, Matsushima M, Suzuki M, Sagae S, Kudo R, Saito J, Noda K, Nakamura Y. Definition of a commonly deleted region in ovarian cancers to a 300-kb segment of chromosome 6q27. Cancer Res 1996;56:5586–9.
10. Tibiletti MG, Bernasconi B, Furlan D, Riva C, Trubia M, Buraggi G, Franchi M, Bolis P, Mariani A, Frigerio L, Capella C, Taramelli R. Early involvement of 6q in surface epithelial ovarian tumors. Cancer Res 1996;56:4493–8.
11. Orphanos V, Mcgown G, Hey Y, Thorncroft M, Santibanez-Koref M, Russell SE, Hickey I, Atkinson RJ, Boyle JM. Allelic imbalance of chromosome 6q in ovarian tumours. Br J Cancer 1995;71:666–9.
12. Rodriguez C, Causse A, Ursule E, Theillet C. At least five regions of imbalance on 6q in breast tumors, combining losses and gains. Genes Chromosomes Cancer 2000;27:76–84.
13. Morita R, Saito S, Ishikawa J, Ogawa O, Yoshida O, Yamakawa K, Nakamura Y. Common regions of deletion on chromosomes 5q, 6q, and 10q in renal cell carcinoma. Cancer Res 1991; 51:5817–20.
14. Kong FM, Anscher MS, Washington MK, Killian JK, Jirtle RL. M6P/IGF2R is mutated in squamous cell carcinoma of the lung. Oncogene 2000;19:1572–8.
15. Picchio MC, Martin ES, Cesari R, Calin GA, Yendamuri S, Kuroki T, Pentimalli F, Sarti M, Yoder K, Kaiser LR, Fishel R, Croce CM, et al. Alterations of the tumor suppressor gene Parkin in non-small cell lung cancer. Clin Cancer Res 2004;10:2720–4.
16. Cesari R, Martin ES, Calin GA, Pentimalli F, Bichi R, Mcadams H, Trapasso F, Drusco A, Shimizu M, Masciullo V, D'andrilli G, Scambia G, et al. Parkin, a gene implicated in autosomal recessive juvenile parkinsonism, is a candidate tumor suppressor gene on chromosome 6q25-q27. Proc Natl Acad Sci USA 2003;100:5956–61.
17. Denison SR, Wang F, Becker NA, Schule B, Kock N, Phillips LA, Klein C, Smith DI. Alterations in the common fragile site gene Parkin in ovarian and other cancers. Oncogene 2003;22:8370–8.
18. Wang F, Denison S, Lai JP, Philips LA, Montoya D, Kock N, Schule B, Klein C, Shridhar V, Roberts LR, Smith DI. Parkin gene alterations in hepatocellular carcinoma. Genes Chromosomes Cancer 2004;40:85–96.
19. Fujiwara M, Marusawa H, Wang HQ, Iwai A, Ikeuchi K, Imai Y, Kataoka A, Nukina N, Takahashi R, Chiba T. Parkin as a tumor suppressor gene for hepatocellular carcinoma. Oncogene 2008;27:6002–11.
20. Schraml P, Bucher C, Bissig H, Nocito A, Haas P, Wilber K, Seelig S, Kononen J, Mihatsch MJ, Dirnhofer S, Sauter G. Cyclin E overexpression and amplification in human tumours. J Pathol 2003;200:375–82.
21. Sutter T, Dansranjavin T, Lubinski J, Debniak T, Giannakudis J, Hoang-Vu C, Dralle H. Overexpression of cyclin E protein is closely related to the mutator phenotype of colorectal carcinoma. Int J Colorectal Dis 2002;17:374–80.
22. Seimi SK, Seinosuke K, Tsuyoshi S, Tomomi U, Tetsuaki H, Miki K, Ryuji T, Kenji I, Mitsuhiro Y. Glycogen synthase kinase-3beta is involved in the process of myocardial hypertrophy stimulated by insulin-like growth factor-1. Circ J 2004;68:247–53.
23. Matsumoto Y, Marusawa H, Kinoshita K, Endo Y, Kou T, Morisawa T, Azuma T, Okazaki IM, Honjo T, Chiba T. Helicobacter pylori infection triggers aberrant expression of activation-induced cytidine deaminase in gastric epithelium. Nat Med 2007;13:470–6.
24. Iwai A, Marusawa H, Matsuzawa S, Fukushima T, Hijikata M, Reed JC, Shimotohno K, Chiba T. Siah-1L, a novel transcript variant belonging to the human Siah family of proteins, regulates beta-catenin activity in a p53-dependent manner. Oncogene 2004;23: 7593–600.
25. Endo Y, Marusawa H, Kinoshita K, Morisawa T, Sakurai T, Okazaki IM, Watashi K, Shimotohno K, Honjo T, Chiba T. Expression of activation-induced cytidine deaminase in human hepatocytes via NF-kappaB signaling. Oncogene 2007;26:5587–95.
26. Sobin LH, Wittekind C. TNM classification of malignant tumor, 6th edn. New York: Wiley, 2002.
27. Normanno N, De Luca A, Bianco C, Strizzi L, Mancino M, Maiello MR, Carotenuto A, De Feo G, Caponigro F, Salomon DS. Epidermal growth factor receptor (EGFR) signaling in cancer. Gene 2006;366:2–16.
28. Yasui W, Sumiyoshi H, Hata J, Kameda T, Ochiai A, Ito H, Tahara E. Expression of epidermal growth factor receptor in human gastric and colonic carcinomas. Cancer Res 1988;48:137–41.
29. Salomon DS, Brandt R, Ciardiello F, Normanno N. Epidermal growth factor-related peptides and their receptors in human malignancies. Crit Rev Oncol Hematol 1995;19:183–232.
30. Cunningham D, Humblet Y, Siena S, Khayat D, Bleiberg H, Santoro A, Bets D, Mueser M, Harstrick A, Verslype C, Chau I, Van Cutsem E, et al. Cetuximab monotherapy and cetuximab plus irinotecan in irinotecan-refractory metastatic colorectal cancer. N Engl J Med 2004;351:337–45.
31. Yang XD, Jia XC, Corvalan JR, Wang P, Davis CG, Jakobovits A. Eradication of established tumors by a fully human monoclonal antibody to the epidermal growth factor receptor without concomitant chemotherapy. Cancer Res 1999;59:1236–43.
32. Kahle PJ, Haass C. How does parkin ligate ubiquitin to Parkinson's disease? EMBO Rep 2004; 5:681–5.
33. Venables JP. Alternative splicing in the testes. Curr Opin Genet Dev 2002;12:615–19.
34. Venables JP. Aberrant and alternative splicing in cancer. Cancer Res 2004;64:7647–54.
35. Srebrow A, Kornblihtt AR. The connection between splicing and cancer. J Cell Sci 2006;119: 2635–41.
36. Stickeler E, Kittrell F, Medina D, Berget SM. Stage-specific changes in SR splicing factors and alternative splicing in mammary tumorigenesis. Oncogene 1999;18:3574–82.
37. Matter N, Herrlich P, Konig H. Signal-dependent regulation of splicing via phosphorylation of Sam68. Nature 2002;420:691–5.
38. Sherr CJ. G1 phase progression: cycling on cue. Cell 1994;79:551–5.
39. Dulic V, Lees E, Reed SI. Association of human cyclin E with a periodic G1-S phase protein kinase. Science 1992;257:1958–61.
40. Koff A, Giordano A, Desai D, Yamashita K, Harper JW, Elledge S, Nishimoto T, Morgan DO, Franza BR, Roberts JM. Formation and activation of a cyclin E-cdk2 complex during the G1 phase of the human cell cycle. Science 1992;257:1689–94.
41. Ekholm SV, Reed SI. Regulation of G(1) cyclin-dependent kinases in the mammalian cell cycle. Curr Opin Cell Biol 2000;12:676–84.
42. Keyomarsi K, Conte D, Toyofuku W, Fox MP. Deregulation of cyclin E in breast cancer. Oncogene 1995;11:941–50.
43. Ohtsubo M, Roberts JM. Cyclin-dependent regulation of G1 in mammalian fibroblasts. Science 1993;259:1908–12.
44. Bedrosian I, Lu KH, Verschraegen C, Keyomarsi K. Cyclin E deregulation alters the biologic properties of ovarian cancer cells. Oncogene 2004;23:2648–57.
45. Akli S, Zheng PJ, Multani AS, Wingate HF, Pathak S, Zhang N, Tucker SL, Chang S, Keyomarsi K. Tumor-specific low molecular weight forms of cyclin E induce genomic instability and resistance to p21, p27, and antiestrogens in breast cancer. Cancer Res 2004;64:3198–208.
46. Spruck CH, Won KA, Reed SI. Deregulated cyclin E induces chromosome instability. Nature 1999;401:297–300.

BRAIN RESEARCH 1294 (2009) 202–210

available at www.sciencedirect.com

ScienceDirect

www.elsevier.com/locate/brainres

BRAIN RESEARCH

Research Report

Chronic cerebral hypoperfusion accelerates amyloid β deposition in APPSwInd transgenic mice

Hiroshi Kitaguchi[a], *Hidekazu Tomimoto*[a,*], *Masafumi Ihara*[a], *Masunari Shibata*[a], *Kengo Uemura*[a], *Rajesch N. Kalaria*[d], *Takeshi Kihara*[c], *Megumi Asada-Utsugi*[b], *Ayae Kinoshita*[b], *Ryosuke Takahashi*[a]

[a]*Department of Neurology, Kyoto University, Sakyo-ku, Kyoto, 606-8504, Japan*

[b]*School of Health Sciences, Graduate School of Medicine, Kyoto University, Sakyo-ku, Kyoto, 606-8504, Japan*

[c]*Department of Neuroscience for Drug Discovery, Graduate School of Pharmaceutical Sciences, Kyoto University, Sakyo-ku, Kyoto, 606-8501, Japan*

[d]*Institute for Health and Ageing, University of Newcastle upon Tyne, Newcastle General Hospital, Westgate Road, Newcastle-upon-Tyne, NE4 6BE, UK*

ARTICLE INFO

Article history:
Accepted 22 July 2009
Available online 30 July 2009

Keywords:
Cerebral ischemia
Amyloid β
Amyloid precursor protein
Transgenic mouse

ABSTRACT

Chronic cerebral ischemia may accelerate clinicopathological changes in Alzheimer's disease. We have examined whether chronic cerebral hypoperfusion accelerates amyloid β deposition in amyloid protein precursor transgenic (APP-Tg) mouse. At 5, 8, and 11 months of age, C57Bl/6J male mice overexpressing a mutant form of the human APP bearing the both Swedish (K670N/M671L) and the Indiana (V717F) mutations (APPSwInd) and their litterrmates were subjected to either sham operation or bilateral carotid artery stenosis (BCAS) using microcoils with an internal diameter of 0.18 mm (short-period group). One month after the sham operation or BCAS, these animals were examined by immunohistochemistry for glial fibrillary acidic protein, amyloid β_{1-40} ($A\beta_{1-40}$), amyloid β_{1-42} ($A\beta_{1-42}$), as well as Western blotting and filter assay for Aβ. Another batch of the littermates of APPSwInd mice were subjected to either sham operation or BCAS at 3 months and were examined in the same manner after survival for 9 months (long-period group). In the BCAS-treated group, the white matter was rarefied and astroglia was proliferated. Amyloid β_{1-40} immunoreactivity was found in a few axons in the white matter after BCAS, whereas $A\beta_{1-42}$ was accumulated in the scattered cortical neurons and the axons at ages of 6 months and thereafter in the short- and long-period groups. In the neuropil, both $A\beta_{1-40}$ and $A\beta_{1-42}$ were deposited in the sham-operated and BCAS-treated mice at ages of 9 and 12 months. There were no differences between the short-period group at ages of 12 months and the long-period group. Filter assay showed an increase of Aβ fibrils in the extracellular enriched fraction. Taken together, chronic cerebral hypoperfusion increased Aβ fibrils and induced Aβ deposition in the intracellular compartment and, therefore, may accelerate the pathological changes of Alzheimer's disease.

* *Corresponding author*. Present address: Department of Neurology, Graduate School of Medicine, Mie University, 2-174 Edobashi, Tsu, 514-8507, Japan. Fax: +81 59 231 5107.
E-mail address: tomimoto@clin.medic.mie-u.ac.jp (H. Tomimoto).

0006-8993/$ – see front matter © 2009 Elsevier B.V. All rights reserved.
doi:10.1016/j.brainres.2009.07.078

1. Introduction

Alzheimer's disease (AD) is a major cause for dementia and has been considered to be a distinct entity from vascular dementia. However, recent pieces of evidence indicate a contribution of chronic cerebral hypoperfusion to the pathogenesis of AD. Indeed, reduction of cerebral blood flow (CBF) has been shown in temporal, parietal, and frontal cortices in the patients with AD (Waldemar et al., 1994; Johnson et al., 1998). This reduction of CBF has been attributed to reduced cerebral metabolism previously and may represent neurovascular coupling in response to an impaired synaptic activity.

However, several lines of evidence indicate dysregulation of regional CBF in AD brains, independent from derangement of synaptic activity. A decrease of CBF is documented even at early stages, indicating a microcirculatory insufficiency before the onset of AD pathology (Prohovnik et al., 1988). In addition, vascular networks in the cerebral cortices of AD patients are damaged and may contribute to the decrease of CBF (De Jong et al., 1997; Farkas et al., 2000; Kitaguchi et al., 2007), although it remains unclear whether these capillary damages are secondary to amyloid β (Aβ) deposition. Finally, in AD brains, there are frequent white matter (WM) lesions and cortical microinfarctions (Suter et al., 2002; Kovari et al., 2007), which are attributed to chronic cerebral hypoperfusion. In concordance with this microvascular derangement in AD, epidemiological data have revealed that vascular factors including mid-life hypertension and hyperlipidemia, diabetes mellitus, apo E4 genotype, are common risks for both AD and vascular dementia (Skoog et al., 1996; Launer et al., 2000; Kalaria, 2002; Kivipelto et al., 2006). Taken together, one can hypothesize that vascular factors and chronic cerebral hypoperfusion may accelerate AD pathology and cognitive decline.

However, there have been no data on whether chronic cerebral ischemia accelerates Aβ deposition in vivo, because the appropriate animal models have not been available. For this purpose, we successfully established a mouse model of chronic cerebral hypoperfusion, which exhibits mild cerebral hypoperfusion for an extended period and subsequently shows WM lesions and working memory deficits (Shibata et al., 2004; Shibata et al., 2007; Nakaji et al., 2006). In the present study, we applied chronic cerebral hypoperfusion to APP-Tg mouse and tested a possible alteration of Aβ metabolism.

2. Results

2.1. Histological stainings and immunohistochemistry

In the BCAS-treated mice at the age of 6 months and later, the WM was rarefied in the corpus callosum, caudoputamen, internal capsule and *anterior commissure* using Klüver-Barrera staining (Figs. 1A and B). However, there were no foci of cerebral infarctions in the cerebral cortices and the hippocampus. Using immunohistochemistry for GFAP, astroglia were much more numerous in the cerebral cortices, hippocampus, and WM such as the corpus callosum in the BCAS-treated mice at ages of 6, 9, and 12 months, as compared to those in the sham-operated mice (Figs. 1C and D).

Amyloid β_{1-40} immunostaining was observed occasionally in the vessel walls at 6 months and thereafter both in the mice with and without chronic cerebral hypoperfusion (Fig. 2A and B), whereas there were no obvious immunoreactivities in the neuronal somata for $A\beta_{1-42}$. There was no specific staining for $A\beta_{1-40}$ and $A\beta_{1-42}$ without the primary antibodies, and in the sections from wild-type mice which were subjected to either sham operation or BCAS. In the BCAS-treated mice at ages of 6, 9, and 12 months, there were neurons intensely immunoreactive for $A\beta_{1-42}$ with perinuclear staining, which may suggest accumulation of the antigen in the Golgi apparatus and multivesicular bodies, as compared to the sham-operated mice (Figs. 2C–H).

The numerical density of neurons with intensely immunoreactive for $A\beta_{1-42}$ were estimated in the representative 10 fields of 0.18 mm^2 from the cerebral cortex either sham-operated or BCAS-treated mice at ages of 12 months. Fig. 3A indicates an increase of these neurons with intense immunoreactivities for $A\beta_{1-42}$. The mouse model of chronic cerebral hypoperfusion does not exhibit focal necrosis or *atrophy* in the gray matter (Shibata et al., 2007). Similarly, in the gray matter, we did not observe any focal necrosis in the present study, but apoptotic cells significantly increased in number in the hippocampal CA1 and cerebral cortices even at ages of 12 months after BCAS (Figs. 3A and B). Therefore, one can postulate that intracellular accumulation of Aβ affects cellular metabolism and may have some relationship to apoptotic cell death, although it remains unclear whether these apoptotic neurons lead to significant reduction of neuronal density.

In the WM, including pencil fibers of the caudoputamen, optic tract and internal capsules, there were varicose fibers that were immunoreactive to antibodies against $A\beta_{1-42}$, whereas those immunoreactive for $A\beta_{1-40}$ were rarely found (Figs. 4A–D). Accumulation of $A\beta_{1-40}$ and $A\beta_{1-42}$ in the neuropil appeared occasionally in mice at the age of 7 months and constantly at 10 months, either with or without chronic cerebral hypoperfusion. With the antibody against $A\beta_{1-42}$, the immunoreactivity appeared as focal deposits surrounded by fibrillary deposits, whereas those for $A\beta_{1-40}$ were restricted to the round focal deposits, although the significance of differential pattern of amyloid deposits remained unclear (Figs. 4E and F). There were no differences in the distribution of $A\beta_{1-40}$ and $A\beta_{1-42}$ between the short-period group at ages of 12 months and the long-period group.

2.2. Western blot and filter assay

BCAS-treated mice showed the tendency to have higher levels of Aβ ($n=3$, $p=0.071$) in the extracellular-enriched brain fraction, as shown in the littermate pairs (a), (b), and (c) in the upper row of Fig. 5A. However, it did not reach statistical significance after correction by β-actin band density.

Next, we tested whether any structural changes in Aβ can be observed in chronic cerebral hypoperfusion with filter assay using ϕ200-nm nitrocellulose membrane, on which only the protein structures larger than 200 nm in diameter can be blotted. To validate the effectiveness of filter assay in specifically detecting Aβ fibrils, Aβ fibrils were prepared from synthetic $A\beta_{1-42}$ in vitro and subjected to filter assay as well as SDS-PAGE followed by the blotting, using anti-total Aβ

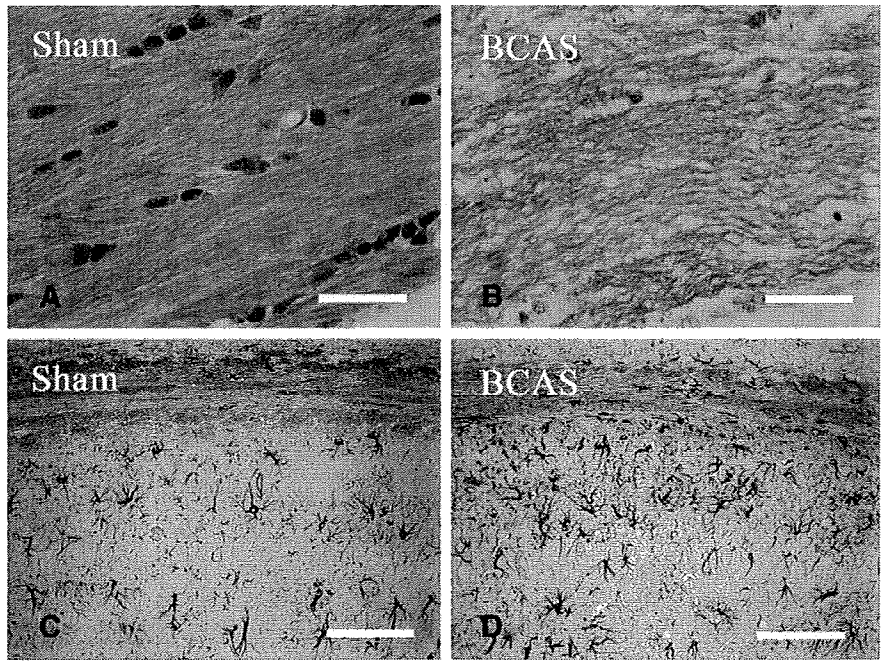

Fig. 1 – Photomicrographs of Klüver-Barrera staining (A, B) and immunohistochemistry for GFAP (C, D) in the corpus callosum (A, B) and the corpus callosum and hippocampal CA1 region (C, D) from the brains of sham-operated mice (A, C) and mice after chronic cerebral hypoperfusion (B, D). All mice were 12 months of age. Note the increase of GFAP-immunoreactive astroglia in both the corpus callosum and hippocampus. Scale bars indicate 50 μm.

(6E10) antibody (Fig. 5B). The Aβ fibrils formed after in vitro incubation were seen as high-molecular weight smear (Fig. 5B, asterisk [*]), which cannot be seen in the Aβ sample without incubation, whereas Aβ oligomers (Fig. 5B, asterisks [**]) and monomer (Fig. 5B, asterisks [***]) were detected with or without incubation. Conversely, in the filter assay, an Aβ-immunoreactive spot was seen only in the sample after incubation (Fig. 5B, bottom), indicating that monomers and oligomers had passed through the membrane.

Thus, we applied filter assay to the extracellular-enriched brain samples from the sham-operated and BCAS-treated mice. Interestingly, the Aβ-immmunoreactive spot density was increased *invariably* in the BCAS-treated mice, compared to the sham-operated mice (Fig. 5C), indicating that Aβ fibril formation was enhanced in the extracellular fraction after BCAS. Quantification of the spot density revealed that the increase was almost by 80% ($p=0.038$, $n=3$, Fig. 5D).

3. Discussion

In previous studies, increase of astroglia has been shown in the cerebral cortex and each part of the white matter in the BCAS-treated mice, along with rarefaction of the white matter (Shibata et al., 2004, 2007). The extent and distribution of glial activation in the present study correspond to those in previous reports and, therefore, indicate the same magnitude of ischemic insults after BCAS.

The altered metabolism of APP and Aβ has been indicated during in vitro hypoxia, and at multiple steps which favor the increase of APP and Aβ. Indeed, in human neuroblastoma cells, chronic hypoxia decreased the levels of α-secretase activity, which may upregulate Aβ production (Webster et al., 2002). In primary culture of neurons from human APP-Tg mice (Tg25769), hypoxia and glucose deprivation increased Aβ with a concomitant increase of γ-secretase and a delayed decrease of α-secretase, ADAM10 (Lee et al., 2006; Marshall et al., 2006). Hypoxia enhances the activity of β-secretase, the rate-limiting enzyme for Aβ production, in the cells expressing human APP695 (Zhang et al., 2007) and facilitates Aβ deposition and neuritic plaque formation in APP-Tg mice (Sun et al., 2006). More recently, neprilysin, metalloproteinase which degrades Aβ, has been shown to decrease in AD (Fisk et al., 2007).

In chronic cerebral ischemia, APP is accumulated in the neurites and soma of affected neurons (Wakita et al., 1992), being enhanced subcellularly in the endopalsmic reticulum and multivesicular bodies after transient global ischemia (Tomimoto et al., 1995). The increased cleavage of Aβ has been shown in a rat model of chronic cerebral hypoperfusion, but tissue deposition has not been demonstrated for Aβ (Bennet et al., 2000). In contrast, in focal cerebral ischemia, dense plaque-like APP deposits appear in the peri-infarct regions (van Groen et al., 2005).

These data collectively indicate that cerebral ischemia induces the abnormal metabolism of Aβ and may replicate the deposition of Aβ in AD. An altered metabolism in Aβ was shown in the present study after chronic cerebral hypoperfuion, but this mechanism remains unclear. β Secretase, β-site APP cleaving (BACE), is a membrane-bound aspartic protease, and the rate-limiting step in Aβ cleavage. Therefore, the Aβ

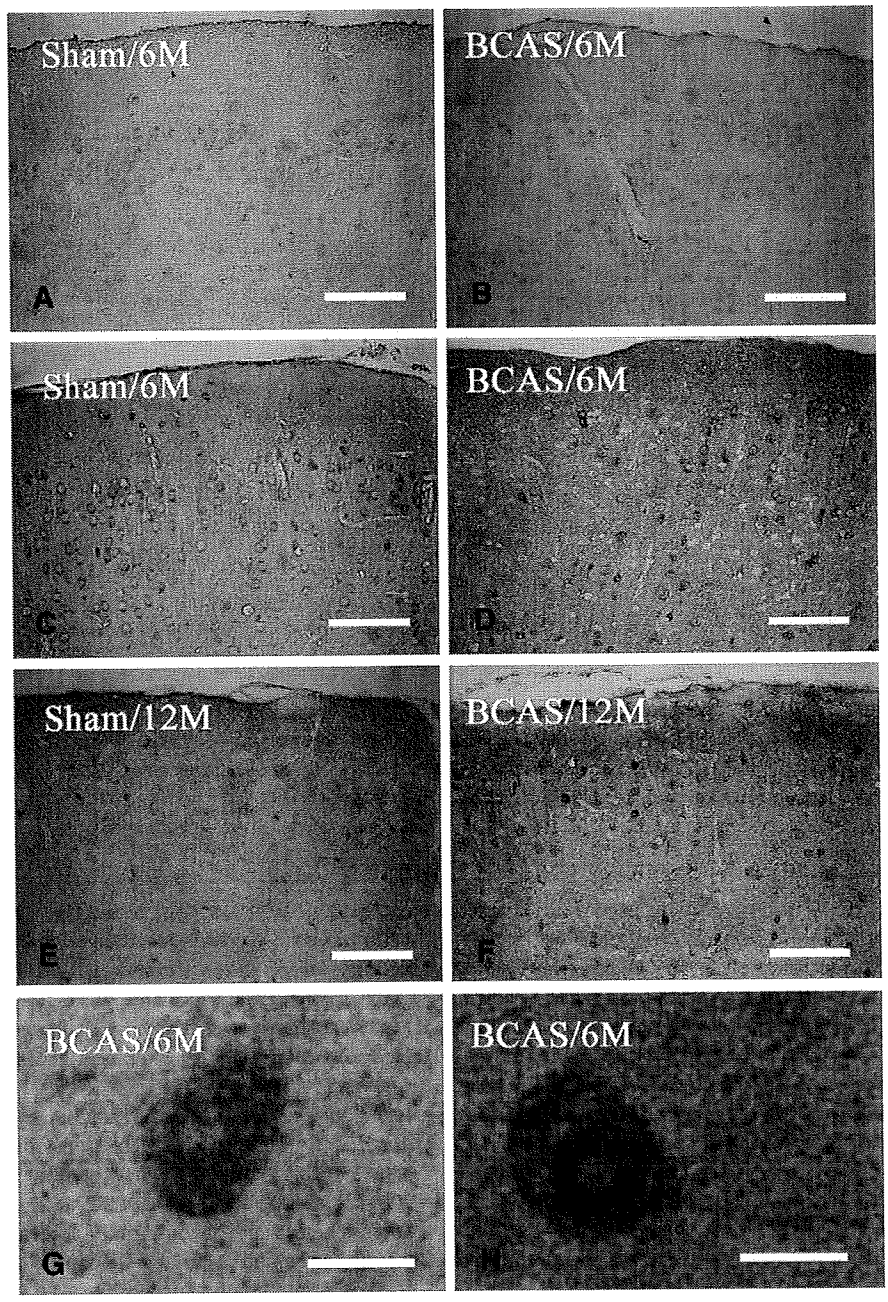

Fig. 2 – Photomicrographs of immunohistochemistry for $A\beta_{1-40}$ (A, B) and $A\beta_{1-42}$ (C–H) in the cerebral cortices. The mice were sham operated (A, C, E) and BCAS treated (B, D, F–H), and sacrificed at 6 months of age (A–D, G, H) and 12 months (E, F). Note that there are scattered intensely immunoreactive neurons, with enhanced immunostaining in the perinuclear regions. These neurons (H) were admixed with the neurons without perinuclear staining (G) in the cerebral cortices of BCAS-treated mice. Scale bars indicate 200 μm (A–F) and 10 μm (G, H).

load has been correlated with an increase in BACE activity in AD (Yang et al., 2003; Li et al., 2004; Chiocco et al., 2004; Johnston et al., 2005; Leuba et al., 2005). In aged APP-Tg mice, BACE was upregulated in the astroglia near amyloid plaques, suggesting that there may be Aβ production in the astroglia (Rossner et al., 2001). More recently, dysregulation in the inter-compartmental transport of soluble Aβ has also been reported in AD with an increase in the receptors for advanced glycation end products (RAGE), thus transporting Aβ into the brain, and a decrease of low-density receptor-related protein (LRP)-1, which transports Aβ outside of the brain (Donahue et al., 2006). Chronic cerebral hypoperfusion may affect each of these processes of Aβ metabolism, and the exact mechanisms should be indicated in the future study.

Finally, it remains to be addressed in the future whether chronic cerebral hypoperfusion induces the abnormal

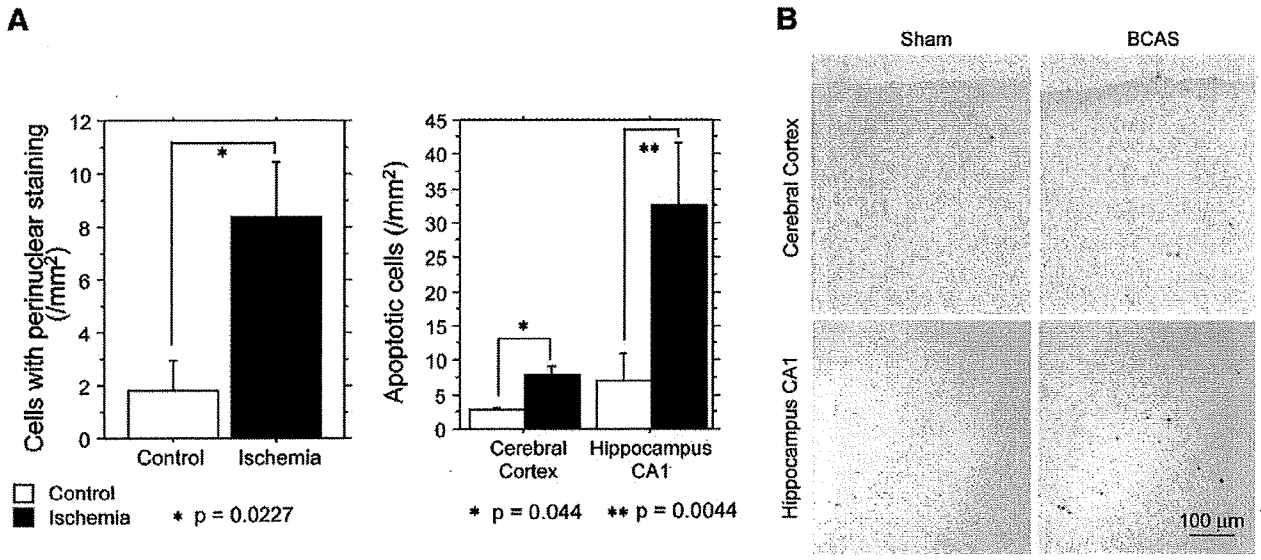

Fig. 3 – (A) Bar graphs showing the numerical density of cells with perinuclear staining and apoptotic cells. (B) Photomicrographs of TUNEL staining in the cerebral cortex and hippocampus in either sham-operated or BCAS-treated mice at 12 months of age.

phosphorylation of tau protein (Ikeda et al., 1998) and consequently accelerates synaptic dysfunction and cognitive deficits, since the Aβ load does not necessarily predict the magnitude of cognitive impairment (Giannakopoulos et al., 2003).

4. Experimental procedures

4.1. *Animals and treatments*

We used human APP-Tg mice overexpressing the familial AD-linked mutation carrying a mutant form of the human APP bearing the both Swedish (K670N/M671L) and the Indiana (V717F) mutations (APP*SwInd*) (Mucke et al., 2000), which has been imported from the Jackson Laboratory (USA). Mice were screened for transgene expression by PCR, and heterozygous mice were mated with nontransgenic C57BL/6J mice. All male heterozygous transgenic mice were given free access to food and water *ad libitum*. All procedures were performed in accordance with the guidelines for animal experimentation from the ethical committee of Kyoto University.

These mice were anesthetized with sodium pentobarbital intraperitoneally. Through a midline cervical incision, both common carotid arteries (CCAs) were exposed and freed from their sheaths. The microcoils, which were made of piano wire with an inner diameter of 0.18 mm, were constructed in Sawane Spring Co. (Japan). This microcoil was twined by rotating around the right CCA. After 30 min, another microcoil was twined around the left CCA. For the sham operation, the CCAs of the animals were exposed, but the microcoils were not twined.

Comparisons were then performed between APP*SwInd* transgenic mice and their littermates. At 5, 8, and 11 months of age, littermates of APP-Tg mice were subjected to either sham operation or bilateral carotid artery stenosis (BCAS) using microcoils (short-period group). One month after the sham operation or BCAS, these animals were examined. To test the effects of duration of chronic cerebral hypoperfusion, another batch of littermates of the APP-Tg mice were subjected to either sham operation or BCAS at 3 months of ages and were examined in the same manner after the survival for 9 months (long-period group). The long-period group was then compared to those operated at 11 months and sacrificed at 12 months.

4.2. *Histopathology and immunohistochemistry*

All animals were euthanized at 1 month and perfused transcardially with 0.01 mol/L phosphate-buffered saline (PBS) followed by 4% paraformaldehyde and 0.2% picric acid in 0.1 mol/L PBS (pH 7.4). The brains were removed and coronal brain blocks were postfixed for 24 h in 4% paraformaldehyde in 0.1 M PBS (pH 7.4) and then stored in 20% sucrose in 0.1 M PB (pH 7.4). Paraffin-embedded tissue was sectioned at 6-μm thickness. These sections were stained with hematoxylin and eosin (H & E) for examination of overall morphology and Klüver-Barrera staining for examination of the WM lesions.

For immunohistochemistry, the paraffin sections were incubated overnight at 4 °C with anti-glial fibrillary acidic protein (GFAP; Dakopatts, Denmark; diluted 1:1000). These sections were incubated with biotinylated anti-mouse IgG (Vector Laboratories, USA; diluted 1:200), and subsequently with avidin-biotin complex solution (Vector Laboratories; diluted 1:100). After each reaction, the sections were rinsed for 15 min with 0.1 M PBS. Finally, the immunoreaction products were visualized with a solution of 0.02% 3, 3′-diaminobenzidine tetrahydrochloride (DAB) and 0.005% H_2O_2 in 0.05 M Tris buffer (pH 7.6). Immunohistochemistry for $A\beta_{1-40}$ and $A\beta_{1-42}$ was performed using Aβ staining kit (Dakoppatts, Denmark) according to the manufacturer's recommendation.

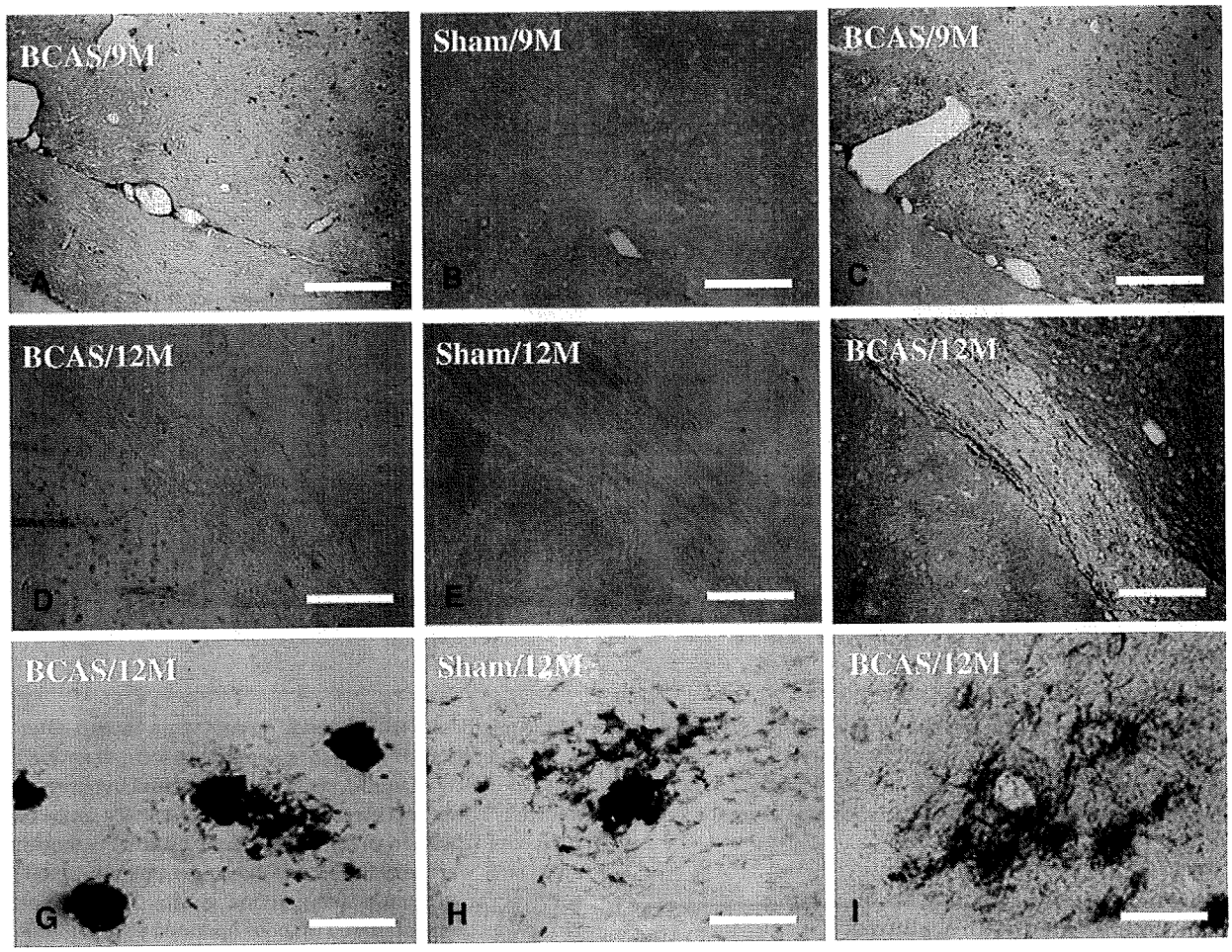

Fig. 4 – Photomicrographs of the immunohistochemistry for $A\beta_{1-40}$ (A, D, G) and $A\beta_{1-42}$ (B, C, E, F, H, I) in the internal capsule and optic tract (A–F) and the hippocampal CA3 region (G–I). Mice were sham treated (B, E, H) and BCAS treated (A, C, D, F, G, I) and sacrificed at 9 months of age (A–C) and 12 months (D–I). Scale bars indicate 500 μm (A–F) and 100 μm (G–I).

TUNEL staining was performed using the Apoptag in situ kit obtained from Oncor (Gaithersberg, MD, USA). After immersion in an equilibration buffer for 5 min, the sections were incubated with TdT and dUTP-digoxigenin in a humidified chamber at 37 °C for 1 h, and then incubated in the stop/wash buffer for 30 min. The sections were washed with 0.1 M PBS and incubated with an anti digoxigenin-peroxidase solution for 30 min. The sections were colorized with DAB-H_2O_2 solution as described above.

4.3. *Protein extraction*

The protein samples for Western blotting and the filter assay were extracted according to the method proposed by Lesne et al. (2006). Briefly, hemi-forebrains were harvested in 500 μL of solution containing 50 mM Tris–HCl (pH 7.6), 1% NP-40, 150 mM NaCl, 2 mM EDTA, 0.1% SDS, 1 mM phenylmethylsulfonyl fluoride (PMSF), and a protease inhibitor cocktail (Sigma, USA). Soluble, extracellular-enriched proteins were collected from mechanically homogenized lysates (1 mL syringe, gauge 20 needle [10 repeats]) following centrifugation for 5 min at 3000 rpm. The protein concentration of the samples was measured according to the Bradford (1976) method and equal amount of protein was subjected to Western blotting or filter assay.

4.4. *Western blotting and filter assay*

To examine the changes of APP metabolism in chronic cerebral hypoperfusion, we extracted the extracellular-enriched proteins from the brains of either sham-operated or BCAS-treated mice according to the protocol by Lesne et al., (2006). These mice were operated at the age of 8 months and sacrificed at the age of 9 months. Three pairs (pairs (a), (b), and (c)) of sham-operated or BCAS-treated mice were used for the analysis. Samples containing equal amounts of protein were diluted by Tricine SDS sample buffer (2×) (Invitrogen, USA) and electrophoresed on a 10%–20% Tricine gel (Invitrogen) in Tricine SDS Running Buffer (Invitrogen) according to the manufacturers' recommendation. Immunoblotting was performed by transferring the proteins to a PVDF membrane, blocking this membrane with 5% skimmed milk in Tris–HCl-buffered saline containing 1% TritonX-100 (TBS-T), and incubated with the primary antibody (6E10, Sigma; diluted

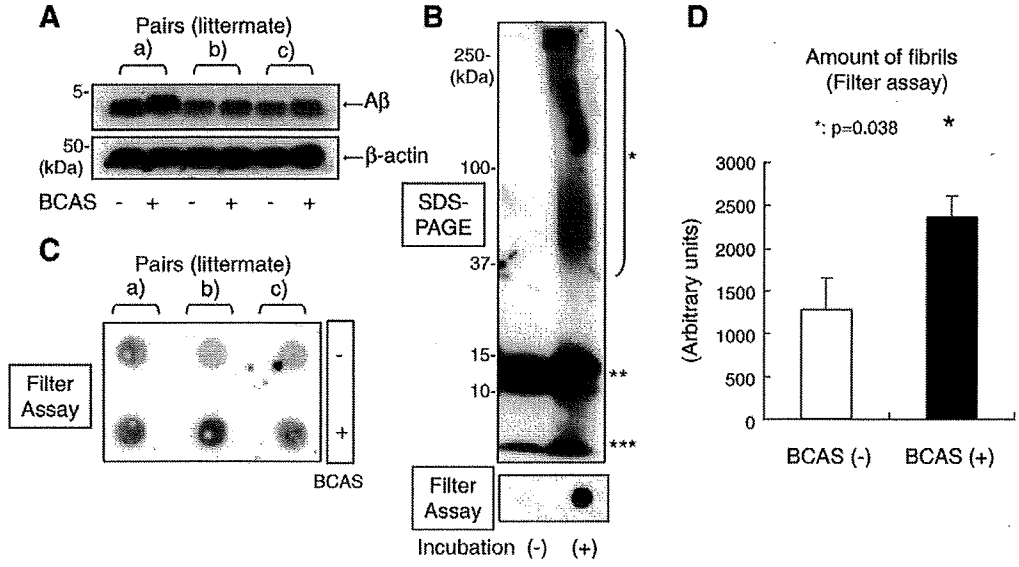

Fig. 5 – (A) Western blot of Aβ in the extracellular-enriched fraction of mouse brains using the anti-total Aβ (6E10) antibody. The lower panel indicates the bands of β-actin, which was used as a loading control. The Aβ fibrils were prepared in vitro from synthetic $A\beta_{1-42}$ and subjected to SDS-PAGE analysis (upper panel). (B) The Aβ fibril was seen as a high-molecular weight smear (*) after incubation. The Aβ oligomers (**) and monomer (***) bands were seen both before and after incubation. The filter assay (bottom panel) demonstrated an Aβ immunopositive spot only after incubation, indicating that the Aβ monomer and oligomers passed through the membrane pore and failed to be blotted onto the membrane. (C) Extracellular-enriched protein samples obtained from brains of either BCAS-treated mice or sham-operated littermates were subjected to the filter assay. The Aβ-immunoreactive spot density was increased in the samples from BCAS-treated mice, as compared to their sham-operated littermates. (D) Statistical analysis of Aβ-immunoreactive spot density. The spot density was significantly increased in the samples obtained the BCAS-treated mice ($p=0.038$, $n=3$).

1:1000) in overnight at 4 °C. The membranes were then incubated with a HRP-linked anti-mouse IgG secondary antibody (GE Healthcare, UK; diluted 1:100) for 1 h at room temperature. The specific reaction was visualized, using the ECL method (GE Healthcare).

Protein samples from the brains of transgenic mice were subjected to vacuum filtration through a 96-well dot blot apparatus (Bio-Rad Laboratories, USA) containing ϕ200-nm nitrocellulose membranes. The resultant membranes were then incubated with primary antibody (6E10; diluted 1:1000) at 4 °C overnight. The membranes were then blocked by TBS-T containing 5% skim milk, and incubated with HRP-linked anti-mouse IgG secondary antibody (GE Healthcare; diluted 1:100) for 1 h. The membranes were developed with the ECL Western Blotting Analysis System (GE Healthcare).

Aβ fibrils for the positive control of the filter assay were prepared from synthetic $A\beta_{1-42}$ (Bachem AG, Switzerland). $A\beta_{1-42}$ was dissolved and brought to 100 μM in 0.1 M HCl and incubated at 37 °C, 24 h, for preparation of fibrils. Control Aβ monomer was dissolved in DMSO (100 μM) and used immediately after preparation. The samples were diluted by PBS into 1 μM and subjected to filter assay.

4.5. *Statistical analysis*

Data were expressed as mean±SEM except when otherwise noted. Statistical analyses were carried out by a one-way ANOVA followed by post hoc Fisher protected least significant differences test. A value of $p<0.05$ was considered statistically significant. Spots density obtained by the filter assay was quantified by the NIH image analyzer. All values are given in means±SD. Comparisons were performed using a paired Student's *t*-test. A $p<0.05$ was considered to indicate a significant difference.

Acknowledgments

This work was supported by a grant-in-aid for scientific research (C) (18590936) from the Japanese Ministry of Education, Culture, Sports and Technology. This study is a part of joint research, which is focusing on the development of the basis of technology for establishing COE for nano-medicine, carried out through Kyoto City Collaboration of Regional Entities for Advancing Technology Excellence assigned by Japan Science and Technology Agency (JST).

REFERENCES

Bennett, S.A., Pappas, B.A., Stevens, W.D., Davidson, C.M., Fortin, T., Chen, J., 2000. Cleavage of amyloid precursor protein elicited by chronic cerebral hypoperfusion. Neurobiol. Aging 21, 207–214.

Bradford, M.M., 1976. A rapid and sensitive method for the quantitation of microgram quantities of protein utilizing the principle of protein-dye binding. Anal. Biochem. 72, 248–254.

Chiocco, M.J., Kulnane, L.S., Younkin, L., Younkin, S., Evin, G., Lamb, B.T., 2004. Altered amyloid-beta metabolism and deposition in genomic-based beta-secretase transgenic mice. J. Biol. Chem. 279, 52535–52542.

De Jong, G.I., De Vos, R.A., Steur, E.N., Luiten, P.G., 1997. Cerebrovascular hypoperfusion: a risk factor for Alzheimer's disease? Animal model and postmortem human studies. Ann. N. Y. Acad. Sci. 826, 56–74.

Donahue, J.E., Flaherty, S.L., Johanson, C.E., Duncan III, J.A., Silverberg, G.D., Miller, M.C., Tavares, R., Yang, W., Wu, Q., Sabo, E., Hovanesian, V., Stopa, E.G., 2006. RAGE, LRP-1, and amyloid-beta protein in Alzheimer's disease. Acta. Neuropathol. (Berl). 112, 405–415.

Farkas, E., De Jong, G.I., Apro, E., De Vos, R.A., Steur, E.N., Luiten, P.G., 2000. Similar ultrastructural breakdown of cerebrocortical capillaries in Alzheimer's disease, Parkinson's disease, and experimental hypertension. What is the functional link. Ann. N. Y. Acad. Sci. 903, 72–82.

Fisk, L., Nalivaeva, N.N., Boyle, J.P., Peers, C.S., Turner, A.J., 2007. Effects of hypoxia and oxidative stress on expression of neprilysin in human neuroblastoma cells and rat cortical neurons and astrocytes. Neurochem. Res. 32, 1741–1748.

Giannakopoulos, P., Herrmann, F.R., Bussiere, T., Bouras, C., Kovari, E., Perl, D.P., Morrison, J.H., Gold, G., Hof, P.R., 2003. Tangle and neuron numbers, but not amyloid load, predict cognitive status in Alzheimer's disease. Neurology 60, 1495–1500.

Ikeda, K., Akiyama, H., Arai, T., Kondo, H., Haga, C., Iritani, S., Tsuchiya, K., 1998. Alz-50/Gallyas-positive lysosome-like intraneuronal granules in Alzheimer's disease and control brains. Neurosci. Lett. 258, 113–116.

Johnson, K.A., Jones, K., Holman, B.L., Becker, J.A., Spiers, P.A., Satlin, A., Albert, M.S., 1998. Preclinical prediction of Alzheimer's disease using SPECT. Neurology 50, 1563–1571.

Johnston, J.A., Liu, W.W., Todd, S.A., Coulson, D.T., Murphy, S., Irvine, G.B., Passmore, A.P., 2005. Expression and activity of beta-site amyloid precursor protein cleaving enzyme in Alzheimer's disease. Biochem. Soc. Trans. 33 (Pt 5), 1096–1100.

Kalaria, R., 2002. Similarities between Alzheimer's disease and vascular dementia. J. Neurol. Sci. 203-204, 29–34.

Kitaguchi, H., Ihara, M., Saiki, H., Takahashi, R., Tomimoto, H., 2007. Capillary beds are decreased in Alzheimer's disease, but not in Binswanger's disease. Neurosci. Lett. 417, 128–131.

Kivipelto, M., Ngandu, T., Laatikainen, T., Winblad, B., Soininen, H., Tuomilehto, J., 2006. Risk score for the prediction of dementia risk in 20 years among middle aged people: a longitudinal, population-based study. Lancet. Neurol. 5, 735–741.

Kovari, E., Gold, G., Herrmann, F.R., Canuto, A., Hof, P.R., Bouras, C., Giannakopoulos, P., 2007. Cortical microinfarcts and demyelination affect cognition in cases at high risk for dementia. Neurology 68, 927–931.

Launer, L.J., Ross, G.W., Petrovitch, H., Masaki, K., Foley, D., White, L.R., Havlik, R.J., 2000. Midlife blood pressure and dementia: the Honolulu-Asia aging study. Neurobiol. Aging 21, 49–55.

Lee, P.H., Hwang, E.M., Hong, H.S., Boo, J.H., Mook-Jung, I., Huh, K., 2006. Effect of ischemic neuronal insults on amyloid precursor protein processing. Neurochem. Res. 31, 821–827.

Lesne, S., Koh, M.T., Kotilinek, L., Kayed, R., Glabe, C.G., Yang, A., Gallagher, M., Ashe, K.H., 2006. A specific amyloid-beta protein assembly in the brain impairs memory. Nature 440, 352–357.

Leuba, G., Wernli, G., Vernay, A., Kraftsik, R., Mohajeri, M.H., Saini, K.D., 2005. Neuronal and nonneuronal quantitative BACE immunocytochemical expression in the entorhinohippocampal and frontal regions in Alzheimer's disease. Dement. Geriatr. Cogn. Disord. 19, 171–183.

Li, R., Lindholm, K., Yang, L.B., Yue, X., Citron, M., Yan, R., Beach, T., Sue, L., Sabbagh, M., Cai, H., Wong, P., Price, D., Shen, Y., 2004. Amyloid beta peptide load is correlated with increased beta-secretase activity in sporadic Alzheimer's disease patients. Proc. Natl. Acad. Sci. U.S.A. 101, 3632–3637.

Marshall, A.J., Rattray, M., Vaughan, P.F., 2006. Chronic hypoxia in the human neuroblastoma SH-SY5Y causes reduced expression of the putative alpha-secretases, ADAM10 and TACE, without altering their mRNA levels. Brain Res. 1099, 18–24.

Mucke, L., Masliah, E., Yu, G.Q., Mallory, M., Rockenstein, E.M., Tatsuno, G., Hu, K., Kholodenko, D., Johnson-Wood, K., McConlogue, L., 2000. High-level neuronal expression of abeta 1-42 in wild-type human amyloid protein precursor transgenic mice: synaptotoxicity without plaque formation. J. Neurosci. 20, 4050–4058.

Nakaji, K., Ihara, M., Takahashi, C., Itohara, S., Noda, M., Takahashi, R., Tomimoto, H., 2006. Matrix metalloproteinase-2 plays a critical role in the pathogenesis of white matter lesions after chronic cerebral hypoperfusion in rodents. Stroke 37, 2816–2823.

Prohovnik, I., Mayeux, R., Sackeim, H.A., Smith, G., Stern, Y., Alderson, P.O., 1988. Cerebral perfusion as a diagnostic marker of early Alzheimer's disease. Neurology 38, 931–937.

Rossner, S., Apelt, J., Schliebs, R., Perez-Polo, J.R., Bigl, V., 2001. Neuronal and glial beta-secretase (BACE) protein expression in transgenic Tg2576 mice with amyloid plaque pathology. J. Neurosci. Res. 64, 437–446.

Skoog, I., Lernfelt, B., Landahl, S., Palmertz, B., Andreasson, L.A., Nilsson, L., Persson, G., Oden, A., Svanborg, A., 1996. 15-year longitudinal study of blood pressure and dementia. Lancet 347, 1141–1145.

Sun, X., He, G., Qing, H., Zhou, W., Dobie, F., Cai, F., Staufenbiel, M., Huang, L.E., Song, W., 2006. Hypoxia facilitates Alzheimer's disease pathogenesis by up-regulating BACE1 gene expression. Proc. Natl. Acad. Sci. U.S.A. 103, 18727–18732.

Suter, O.C., Sunthorn, T., Kraftsik, R., Straubel, J., Darekar, P., Khalili, K., Miklossy, J., 2002. Cerebral hypoperfusion generates cortical watershed microinfarcts in Alzheimer disease Stroke 33, 1986–1992.

Shibata, M., Ohtani, R., Ihara, M., Tomimoto, H., 2004. White matter lesions and glial activation in a novel mouse model of chronic cerebral hypoperfusion. Stroke 35, 2598–2603.

Shibata, M., Yamasaki, N., Miyakawa, T., Kalaria, R.N., Fujita, Y., Ohtani, R., Ihara, M., Takahashi, R., Tomimoto, H., 2007. Selective impairment of working memory in a mouse model of chronic cerebral hypoperfusion. Stroke 38, 2826–2832.

Tomimoto, H., Akiguchi, I., Wakita, H., Nakamura, S., Kimura, J., 1995. Ultrastructural localization of amyloid protein precursor in the normal and postischemic gerbil brain. Brain Res. 672, 187–195.

van Groen, T., Puurunen, K., Maki, H.M., Sivenius, J., Jolkkonen, J., 2005. Transformation of diffuse beta-amyloid precursor protein and beta-amyloid deposits to plaques in the thalamus after transient occlusion of the middle cerebral artery in rats. Stroke 36, 1551–1556.

Wakita, H., Tomimoto, H., Akiguchi, I., Ohnishi, K., Nakamura, S., Kimura, J., 1992. Regional accumulation of amyloid beta/A4 protein precursor in the gerbil brain following transient cerebral ischemia. Neurosci. Lett. 146, 135–138.

Waldemar, G., Bruhn, P., Kristensen, M., Johnsen, A., Paulson, O.B., Lassen, N.A., 1994. Heterogeneity of neocortical cerebral blood flow deficits in dementia of the Alzheimer type: a [99mTc]-d, l-HMPAO SPECT study. J. Neurol. Neurosurg. Psychiatry 57, 285–295.

Webster, N.J., Green, K.N., Peers, C., Vaughan, P.F., 2002. Altered processing of amyloid precursor protein in the human neuroblastoma SH-SY5Y by chronic hypoxia. J. Neurochem. 83, 1262–1271.

Yang, L.B., Lindholm, K., Yan, R., Citron, M., Xia, W., Yang, X.L., Beach, T., Sue, L., Wong, P., Price, D., Li, R., Shen, Y., 2003. Elevated beta-secretase expression and enzymatic activity detected in sporadic Alzheimer disease. Nat. Med. 9, 3–4.

Zhang, X., Zhou, K., Wang, R., Cui, J., Lipton, S.A., Liao, F.F., Xu, H., Zhang, Y.W., 2007. Hypoxia-inducible factor 1alpha (HIF-1alpha)-mediated hypoxia increases BACE1 expression and beta-amyloid generation. J. Biol. Chem. 282, 10873–10880.

INTERNAL MEDICINE

□ CASE REPORT □

Leukoencephalopathy with Cognitive Impairment following Tocilizumab for the Treatment of Rheumatoid Arthritis (RA)

Katsuya Kobayashi[1], Yoko Okamoto[1], Haruhisa Inoue[1], Takashi Usui[2], Masafumi Ihara[1], Jun Kawamata[1], Yukio Miki[3], Tsuneyo Mimori[2], Hidekazu Tomimoto[4] and Ryosuke Takahashi[1]

Abstract

The biological agent tocilizumab, is a humanized, anti-human interleukin-6 receptor antibody. A 72-year-old woman developed cognitive impairment during the Phase III clinical trial of tocilizumab for the treatment of rheumatoid arthritis. MRI demonstrated hyperintense dissemination throughout the white matter on T2WI. An initial diagnosis of possible progressive multifocal leukoencephalopathy was made, but the PCR for JC virus DNA was negative in the CSF. The leukoencephalopathy might have been caused by a mechanism related to tocilizumab itself. It is strongly recommended to perform MRI if a patient develops any cognitive impairment during tocilizumab therapy.

Key words: rheumatoid arthritis, tocilizumab, leukoencephalopathy, cognitive impairment, MRI, interleukin 6

(Inter Med 48: 1307-1309, 2009)
(DOI: 10.2169/internalmedicine.48.1926)

Introduction

Tocilizumab is a humanized, anti-human interleukin-6 receptor antibody, produced by genetic engineering technology. To date, it has been prescribed solely to patients with Castleman disease. Phase III clinical trials of tocilizumab have already been performed on patients with rheumatoid arthritis. Here, we report the first case of leukoencephalopathy with cognitive impairment, likely caused by tocilizumab for the treatment of rheumatoid arthritis.

Case Report

A left-handed 72-year-old woman was referred to our hospital because her cognition had worsened over the previous two months. She had suffered from rheumatoid arthritis (RA) for the past six years, and since a daily dosage of 10 mg prednisolone had not been proved effective, it was decided that she participated in the Phase III clinical trial of tocilizumab. During the trial, the patient took 8 mg/kg of tocilizumab every four weeks. Forty months after commencing to take tocilizumab, she began to show signs of dementia and abnormal behavior. She became unable to check blood glucose by herself, put things in order, and speak coherently.

At the time she was admitted, her blood pressure was 124/64 mmHg, and her body temperature was 37.2℃. A physical examination revealed bilateral pretibial edema and ankylosis of several joints. She was orientated, but anxious and nervous. She was not able to concentrate, and showed cognitive dysfunction with a Mini-Mental State Examination (MMSE) score of 23 and a Frontal Assessment Battery (FAB) score of 8. Snout reflex and bilateral sucking reflexes were positive. There were no motor or sensory disturbances. Bilateral Achilles tendon reflexes were decreased. Laboratory investigation demonstrated normal blood cell counts.

[1]Department of Neurology, Kyoto University Hospital, Kyoto, [2]Department of Rheumatology and Clinical Immunology, Kyoto University Hospital, Kyoto, [3]Department of Diagnostic Imaging and Nuclear Medicine, Kyoto University Hospital, Kyoto and [4]Department of Neurology, Mie University Hospital, Tsu
Received for publication December 7, 2008; Accepted for publication March 22, 2009
Correspondence to Dr. Yoko Okamoto, yoko416@kuhp.kyoto-u.ac.jp

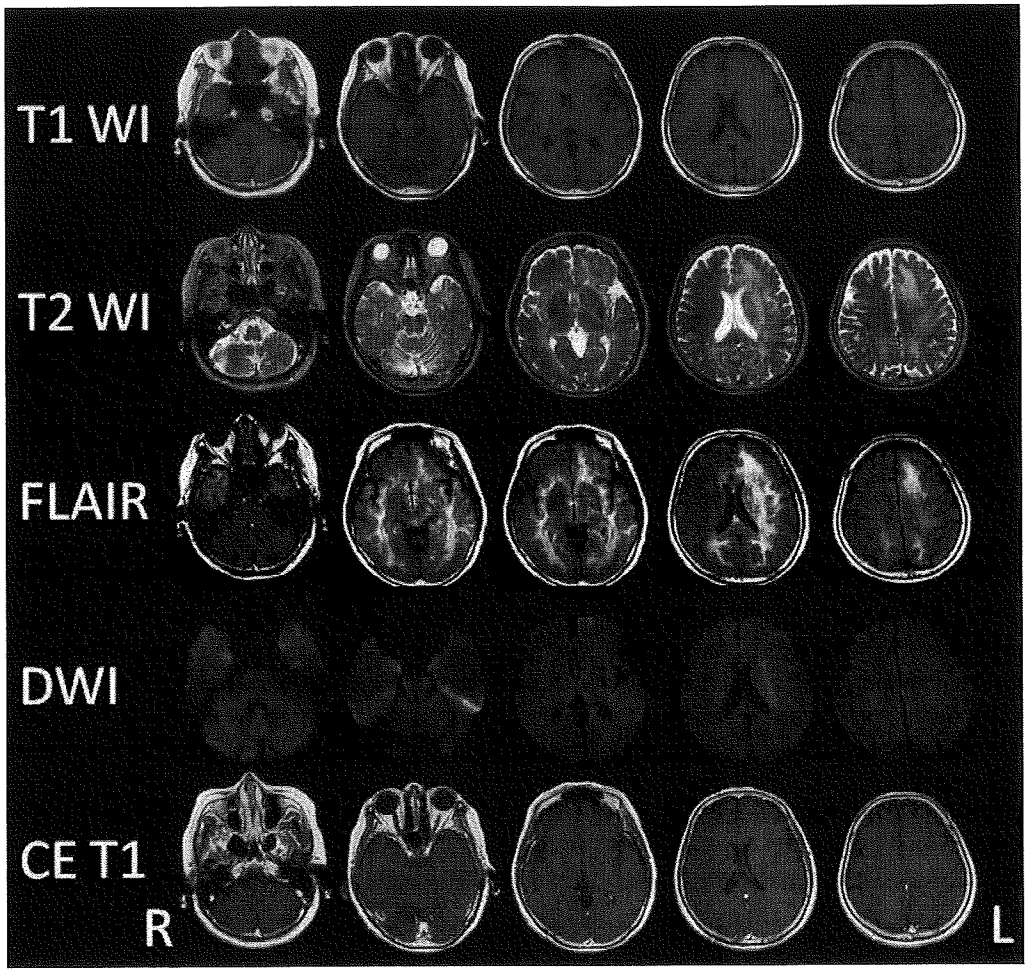

Figure 1. **Brain MRI at the time of the admission. MRI disclosed high intensity dissemination throughout the white matter which spread widely from the temporal tip to the pars opercularis on T2WI and FLAIR. In accordance with the high intensity lesions on T2WI and FLAIR, slightly low intensity lesions were found on T1WI. There was no high intensity lesion on DWI except for T2 "shine-through" lesions of the left corona radiata. There was no mass effect or contrast enhancement lesion on contrast-enhanced T1WI.**

Serum biochemistry showed an elevation of HbA1c (6.2%), anti-nuclear antibody, rheumatoid factor (RF, 62.3 IU/mL) and matrix metalloprotainase-3 (MMP-3, 215 ng/mL). The other autoimmune antibodies including anti-double stranded DNA, ribonucleoprotein, SS-A, SS-B, Scl-70, Jo-1, c-ANCA, p-ANCA, thyroid peroxidase (TPO), and thyroglobulin (TG) antibodies were all negative. Anti HTLV-I and HIV antibodies were also negative. Thyroid hormone, vitamins, angiotensin-converting enzyme (ACE), and anti-soluble interleukin 2 receptor antibodies were within normal limits. The cerebrospinal fluid (CSF) revealed a leukocyte count of 2 /μL, a protein level of 46.6 mg/dL and a glucose level of 61 mg/dL. IgG index elevated to 0.77 and a polymerase chain reaction for JC virus DNA was negative in the CSF.

A brain CT scan demonstrated diffuse low density in the bilateral cerebral white matter. An MRI disclosed high intensity disseminated throughout the white matter which spread widely from the temporal tip to the pars opercularis (Fig. 1). There was no mass effect or contrast enhancement. On the scout view film of the cervical CT checked 6 months earlier, the low density area in the temporal tip and the frontal white matter was already present.

The background activity of electroencephalography consisted of 8-9 Hz, which suggested moderate dysfunction with left dominance. SPECT showed decreased uptake in accordance with the lesions observed in MRI. Although tocilizumab had been discontinued for the previous 5 months, her cognitive function and MRI findings did not change.

Discussion

The patient developed cognitive impairment in the course of tocilizumab therapy for RA. There are various pathoetiologies which may cause diffuse leukoencephalopathy, including collagen disease, vasculitis, reversible posterior leukoencephalopathy syndrome (RPLS), Binswanger disease, isolated angiitis of the central nervous system (CNS), pro-

gressive multifocal leukoencephalopathy (PML), malignant lymphoma, gliomatosis cerebri, and radiation necrosis (1). The serum autoimmune antibodies examined were all negative and the JC virus DNA in the CSF was negative. The MRI showed asymmetrical white matter lesion and no mass effect, contrast enhancement, or cortical lesions. Thus, we could not obtain any supportive evidence for the diagnosis except the probable relevance with tocilizumab. However, the possibility of infection could not be entirely excluded during the hospitalization; therefore immunological therapy was not given.

Drug-induced leukoencephalopathy has been reported on amphotericin B, acyclovir, methotrexate, fluorouracil, tacrolimus, ciclosporin, etc (2). Also, biological agents, such as etanercept, infliximab, rituximab, or natalizmab cause leukoencephalopathy (3-6). Therefore, we postulated that tocilizumab caused the leukoencephalopathy via immunological mechanisms relating to direct and/or indirect IL-6 signaling. When we consider the concrete mechanism, this patient was aged, hypertensive, and undergoing steroid therapy. These factors might cause a synergistic effect on blood brain barrier (BBB) leading to leukoencephalopathy. Once BBB is disrupted, tocilizumab may also spread to the brain parenchyma and suppress IL-6 related glial survival. In fact, direct injection of IL-6 into the brain can reduce ischemic brain injury, though its mechanism is unknown to date (7).

It remains unknown why the leukoencephalopathy was not resolved after tocilizumab discontinuation. One of the plausible explanations is that the leukoencephalopathy had been so advanced and irreversible that symptomatic relief was not obtained. As mentioned above, because the patient was aged, hypertensive, and undergoing steroid therapy, these backgrounds might have some effects on her irreversible symptoms. The pathological changes might be irreversible demyelination or chronic ischemic changes; however, further study is necessary.

This is the first report regarding the development of leukoencephalopathy during the administration of tocilizumab. Therefore, during tocilizumab therapy, it is strongly recommended to conduct a brain MRI if the patient develops any cognitive impairment.

References

1. Hinchey J, Chaves C, Appignani B, et al. A reversible posterior leukoencephalopathy syndrome. N Engl J Med **334**: 494-500, 1996.
2. Shimono T, Miki Y, Toyoda H, et al. MR imaging with quantitative diffusion mapping of tacrolimus-induced neurotoxicity in organ transplant patients. Eur Radiol **13**: 986-993, 2003.
3. Yamamoto M, Takahashi H, Wakasugi H, et al. Leukoencephalopathy during administration of etanercept for refractory rheumatoid arthritis. Mod Rheumatol **17**: 72-74, 2007.
4. Roos JC. Neurological complication of infliximab. J Rheumatol **34**: 236-237, 2007.
5. US Food and Drug Administration. FDA alert: rituximab (marketed as Rituxan). December 2006.
6. Van Assche G, Van Ranst M, Sciot R, et al. Progressive multifocal leukoencephalopathy after natalizumab therapy for Crohn's disease. N Engl J Med **353**: 362-368, 2005.
7. Suzuki S, Tanaka K, Suzuki N. Ambivalent aspects of interleukin-6 in cerebral ischemia: inflammatory versus neurotrophic aspects. J Cereb Blood Flow Metab **29**: 464-479, 2009.

Neuroscience Research 65 (2009) 263–271

Contents lists available at ScienceDirect

Neuroscience Research

journal homepage: www.elsevier.com/locate/neures

A chemical neurotoxin, MPTP induces Parkinson's disease like phenotype, movement disorders and persistent loss of dopamine neurons in medaka fish

Hideaki Matsui [a,c], Yoshihito Taniguchi [b,c], Haruhisa Inoue [a,c], Kengo Uemura [a,c], Shunichi Takeda [b,c,*], Ryosuke Takahashi [a,c,**]

[a] Department of Neurology, Kyoto University, Graduate School of Medicine, Kyoto 606-8507, Japan
[b] Department of Radiation Genetics, Kyoto University, Graduate School of Medicine, Kyoto 606-8501, Japan
[c] Core Research for Evolutional Science and Technology (CREST), Japan Science and Technology Agency, Japan

ARTICLE INFO

Article history:
Received 16 May 2009
Received in revised form 25 June 2009
Accepted 30 July 2009
Available online 7 August 2009

Keywords:
Parkinson's disease
MPTP
Medaka (*Oryzias latipes*)
Movement disorder
Dopamine
Tyrosine hydroxylase

ABSTRACT

Parkinson's disease (PD) is the second most common neurodegenerative disease associated with the degeneration of dopaminergic neurons in the substantia nigra. To create a new model of PD, we used medaka (*Oryzias latipes*), a small teleost that has been used in genetics and environmental biology. We identified tyrosine hydroxylase (TH) immunopositive dopaminergic and noradrenergic fibers and neurons in the medaka brain. Following establishment of a method for counting the number of dopaminergic neurons and an assay for the evaluation of the medaka behavior, we exposed medaka to 1-methyl-4-phenyl-1,2,3,4-tetrahydropyridine (MPTP). The treatment of medaka at the larval stage, but not at adult stage, decreased the number of dopaminergic cells in the diencephalon and reduced spontaneous movement, which is reminiscent of human PD patients and other MPTP-induced animal PD models. Among TH^+ neurons in the medaka brain, only a specific cluster in the paraventricular area of the middle diencephalon was vulnerable to MPTP toxicity. Detailed examinations of medaka transiently exposed to MPTP at the larval stage revealed that the number of dopaminergic cells was not fully recovered at their adult stage. Moreover, the amounts of dopamine persistently decreased in the brain of these MPTP-treated fish. MPTP-treated medaka is valuable for modeling human PD.

1. Introduction

Parkinson's disease (PD) is characterized by the late-onset degeneration of dopaminergic neurons in a subset of neuronal populations represented by the substantia nigra pars compacta in the midbrain. A small proportion of PD is caused by genetic disorder, which provides invaluable insights into the pathogenesis of sporadic PD (Gasser, 2005). Familial PD is caused by autosomal dominant mutations in the genes encoding *α-synuclein* (Polymeropoulos et al., 1997) and *LRRK2* (Paisán-Ruíz et al., 2004; Zimprich et al., 2004), while juvenile parkinsonism is associated with recessive mutations in the genes encoding *parkin* (Kitada et al., 1998), *DJ-1* (Bonifati et al., 2003), and *PINK1* (Rogaeva et al., 2004; Valente et al., 2004). Various models have been developed in several species in order to understand the mechanisms underlying the pathogenesis of PD, including mouse (Bové et al., 2005; Fleming et al., 2005), *Drosophila* (Cauchi and van den Heuvel, 2006), *Caenorhabditis elegans* (van Ham et al., 2008) and yeasts (Outeiro and Lindquist, 2003). However, the pathogenesis of PD remains largely unknown.

Small laboratory fish such as zebrafish (*Danio rerio*) and Japanese medaka (*Oryzias latipes*) are attractive vertebrate animal models, because they are easy to handle and produce large numbers of progeny per generation (Wittbrodt et al., 2002). Medaka is a small aqueous fish that inhabits Asia and has been used as a model organism since early 1900s (Aida, 1921). It has several advantages over zebrafish or goldfish in modeling PD. First, the whole genome has been sequenced and assembled since the size of medaka genome is only 700 Mb, half the size of the zebrafish genome (Kasahara et al., 2007). Second, several inbred strains have been established in medaka, but not in zebrafish. The lack of genetic variations among individuals may simplify and facilitate genetic studies, and is particularly important for disease models. The goldfish is not suitable for genetic research because it does not have good genetic information nor technology for genetics, while most techniques that are used for zebrafish studies are applicable to medaka. Third, the body of medaka is more transparent than

* Corresponding author at: Department of Radiation Genetics, Kyoto University, Graduate School of Medicine, Yoshida-Konoe-cho, Sakyo-ku, Kyoto 606-8501, Japan. Tel.: +81 75 753 4410; fax: +81 75 753 4419.
** Corresponding author at: Department of Neurology, Kyoto University, Graduate School of Medicine, 54 Shogoin-Kawahara-cho, Sakyo-ku, Kyoto 606-8507, Japan. Tel.: +81 75 751 3770; fax: +81 75 751 9780.
E-mail addresses: stakeda@rg.med.kyoto-u.ac.jp (S. Takeda), ryosuket@kuhp.kyoto-u.ac.jp (R. Takahashi).

0168-0102/$ – see front matter © 2009 Elsevier Ireland Ltd and the Japan Neuroscience Society. All rights reserved.
doi:10.1016/j.neures.2009.07.010

that of the zebrafish or goldfish, and it is easy to visualize the *in vivo* target structures. Fourth, cryopreservation of the sperm is easy and reliable, so we can maintain and store numerous strains in the laboratory (Yang and Tiersch, 2009). Finally and most importantly, we have already retrieved PD-related mutants including *parkin* from our TILLING (Targeting Induced Local Lesions IN Genomes) library of medaka (Taniguchi et al., 2006).

1-Methyl-4-phenyl-1,2,3,4-tetrahydropyridine (MPTP) is a neurotoxin that induces PD-like symptoms. It is metabolized in glial cells to 1-methyl-4-phenylpyridinium (MPP^+), and is subsequently incorporated by dopaminergic neurons via dopamine transporter, thereby selectively damaging the dopaminergic neurons through inhibiting the activity of the mitochondria respiratory chain (Gerlach et al., 1991). It has been widely used to generate zebrafish and goldfish model of PD together with other neurotoxins such as 6-hydroxydopamine and rotenone (Pollard et al., 1992; Anichtchik et al., 2004; Wen et al., 2008; Bretaud et al., 2004; Lam et al., 2005; McKinley et al., 2005). However, these studies mainly focus on the acute or subacute effects of neurotoxins on zebrafish or goldfish. One caveat is that the adult neurogenesis occurs extensively in the brain of fish and that neurons are added continuously to various brain regions (Grandel et al., 2006). Therefore, it is important to examine the consequences of MPTP-induced brain lesions over a long period of time in the research using fish. In this study, we report the long-term effect of MPTP on medaka dopaminergic system evaluated by several assays including histological analysis of dopaminergic neurons and the behavioral tests.

2. Materials and methods

2.1. Fish maintenance

Wild-type medaka of *Kyoto-cab* strain was maintained at 27 °C in a recirculating aquaculture system equipped with carbon filtration, ultraviolet light sterilizers and biofiltration. Adult fish were kept under a reproduction regimen (14 h light/10 h dark). Eggs were kept in a dark box at 28 °C.

2.2. MPTP treatment

The MPTP-hydrochloride (Sigma–Aldrich, MO, USA) was dissolved in distilled water to 10 mg/ml. Safety precautions included the use of protective clothing, globes, goggles, masks and decontamination of all surfaces and solutions with 1% bleach at the end of each experiment. For exposure of adult fish, three fish (90-dpf) were kept in 100 ml of water each containing different concentration of MPTP. The water was changed and MPTP was freshly added to the water every week. Three weeks after treatment, the fish was rinsed seven times for total clearance of MPTP and subjected to the analysis (Fig. 2A). For exposure of larvae, five 10-dpf larvae were kept in a cup containing 50 ml water with various concentration of MPTP. Two days after treatment, MPTP was removed and the fish were used for the analysis (Fig. 2B). We used littermates in a series of experiments and all the experiments were done at least twice.

2.3. High performance liquid chromatography

Brain was homogenized in 100 μl of 0.4 M $HClO_4$ containing 4 mM $Na_2S_2O_5$ and 4 mM diethylenetriaminepentaacetic acid. The supernatant by centrifugation at 18,500 × *g* for 5 min was used for measurement of free catechols. High performance liquid chromatography (HPLC) was conducted with a mobile phase containing bufferA:acetonitrile:methanol = 1000:25.9:62.9 (v/v/v) (bufferA: 0.1 M phosphate, 0.05 M citrate, 4 mM sodium 1-heptanesulfonate and 0.1 mM EDTA, pH 3.0). Dopamine and metabolites were detected with series coulometric detector (ESA, Inc., Chelmsford, MA, USA). Data were collected and processed on a CHROMELEON™ Chromatography Data Systems 6.40 (Dionex, Sunnyvale, CA, USA). The pellet was then reserved for the analysis of the protein content. For this purpose, the pellet was solubilized in 100 μl of 0.5 N NaOH at 60 °C and the protein was quantified by the BCA assay method, using bovine serum albumin (BSA) as the standard.

2.4. Immunohistochemistry

After organs were examined under the stereomicroscope, fish were fixed in 4% paraformaldehyde for 24 h and embedded in paraffin. Each brain was sectioned at 20-μm thickness and incubated with mouse anti-tyrosine hydroxylase (TH) antibody (Millipore, MA, USA, 1:500) for 1 h. Immunoperoxidase detection was carried out by using Vector Elite ABC kit with DAB (Vector Laboratories, CA, USA) on every section. The number of dopaminergic neurons in the diencephalon was determined by counting the nucleus of TH^+ neurons in coronal sections using OLYMPUS BX51 microscope with MICROFIRE digital camera (Olympus, Japan) and Stereo Investigator (MBF Bioscience, VT, USA). Photographs were taken by the same equipments. Whole mount immunohistochemistry of larvae was carried out as previously described (Shimamura and Takeichi, 1992). Mouse anti-TH antibody (Millipore, MA, USA, 1:100) was detected via fluorescence using anti-mouse IgG conjugated with Alexa Fluor 546 (Invitrogen, WI, USA). Images were acquired by LSM510 microscope (Carl Zeiss, Germany) and subjected to quantitative analysis using Photoshop (Adobe, CA, USA).

2.5. Western blotting

Brains were homogenized in RIPA buffer (25 mM Tris–HCl pH 7.6, 150 mM NaCl, 1% NP-40, 1% sodium deoxycholate, 0.1% SDS) with protease inhibitors and processed for SDS-PAGE. Immunoreactive bands were detected with ECL reagent or ECL plus reagent (GE Healthcare Life Sciences, Japan) and chemiluminescent signal was visualized by the exposing membrane to Fuji RX-U X-ray film (Fuji Film, Japan). Films were scanned and densitometric analysis of blots was performed using ImageJ software (National Institute of Health). The background intensity of the film was subtracted from the band intensity. Anti-TH monoclonal antibody (1:1000, mouse anti-TH, MAB318, Millipore) was used for the western blotting analysis of TH. For the loading control, anti-β-actin monoclonal antibody (1:5000, AC-15, Sigma–Aldrich) was used.

2.6. Behavioral analysis

Fish were subjected to a spontaneous swimming measuring test during a light phase. Images were collected by a video camera positioned above the water tank under a low indirect dimly white light, and analyzed by a computer-assisted system (Muromachi Kikai, Japan). The water tank was a transparent circular field (2 cm water depth, 27 °C) with the diameter of 5 cm for larvae and 20 cm for adults. We started to acquire the images 1 min after the larvae was entered into the water tank. Adult medaka is more wary of environmental changes compared to zebrafish and larval medaka, and they tend to remain stationary when put in a new tank. We started to acquire the images 1 min after the adult fish began to move in a new water tank. Beginning of this movement was automatically defined when fish moved from one section to another section (Fig. 5D). The data were collected for 1 or 5 min for larvae and adults, respectively. The larvae and adults were judged as they were swimming only when the moving speed exceeded 0.025 cm/0.1 s and 0.1 cm/0.1 s, respectively. Total swimming distance, frequency of swimming movement (duration of swimming movement divided by the total time of observation), and swimming velocity (total swimming distance divided by duration of swimming movement) were measured and compared among the groups.

2.7. Statistical analysis

Data were expressed as mean ± standard error of the mean (SEM). The results were statistically evaluated for significance by applying ANOVA with post hoc analysis using Dunnett's test. Differences were considered significant when $p < 0.05$.

3. Results

3.1. Distribution of dopaminergic neurons in the brain of adult medaka

To examine the distribution of dopaminergic neurons in medaka brain, we used immunohistochemistry of TH to visualize dopaminergic neurons. We identified TH immunopositive (TH^+) fibers in the telencephalon (Fig. 1B). This TH^+ structure in the teleost brain is relevant to the striatum in the human brain (Rink and Wullimann, 2004). Medaka TH^+ neurons aligned from the telencephalon to the diencephalon along the ventro-medial side of the brain (Fig. 1C–F). In the rostral part of diencephalon, clusters of small neurons were found in both dorsal and ventral areas (Fig. 1D). Large TH^+ neurons were distributed towards the caudal area around the ventricle in the middle diencephalon (Fig. 1E). The rostro-ventral TH cluster was around the nucleus posterioris periventricularis (NPPv) and the middle one around the NPPv and the nucleus anterior tuberis. At the most caudal part of the diencephalon, there were small neurons on the dorsal side (Fig. 1F). This cluster existed around the nucleus posterior thalami. We could easily distinguish these clusters because the size of neurons

in each cluster was different and these clusters were clearly separated anatomically from each other. We also detected TH$^+$ noradrenergic neurons in the medulla oblongata (Fig. 1G).

The distribution of TH$^+$ neurons in the medaka diencephalon largely matched with previously published data on zebrafish TH$^+$ neurons and medaka neurons that exhibit *Nurr1* mRNA (Rink and Wullimann, 2004; Kapsimali et al., 2001). Histological examination using retrograde tracers suggests that a subset of dopaminergic neurons in the diencephalon of zebrafish project to the striatum-like structure and may be equivalents of the substantia nigra neurons in mammals (Rink and Wullimann, 2004). For the subsequent experiments in this study, we counted only the number of dopaminergic neurons in the diencephalic clusters because these will contain an equivalent of the substantia nigra. TH$^+$ neurons in the middle diencephalon show a distinct morphology with the large cell body and the intense cytoplasmic staining hollowed by a clear nucleus (Supplementary Fig. 1). There are 87.5 ± 5.6 (n = 8) of such cells in around 200 μm in the paraventriclular area of the middle diencephalon (Fig. 3C). In the rostral and caudal regions to this area, we found 145.9 ± 9.1 and 81.9 ± 8.0 TH$^+$ neurons, respectively, with a smaller cell body (Fig. 3C). Counting these cells yielded highly reproducible data. We also counted the number of TH$^+$ neurons

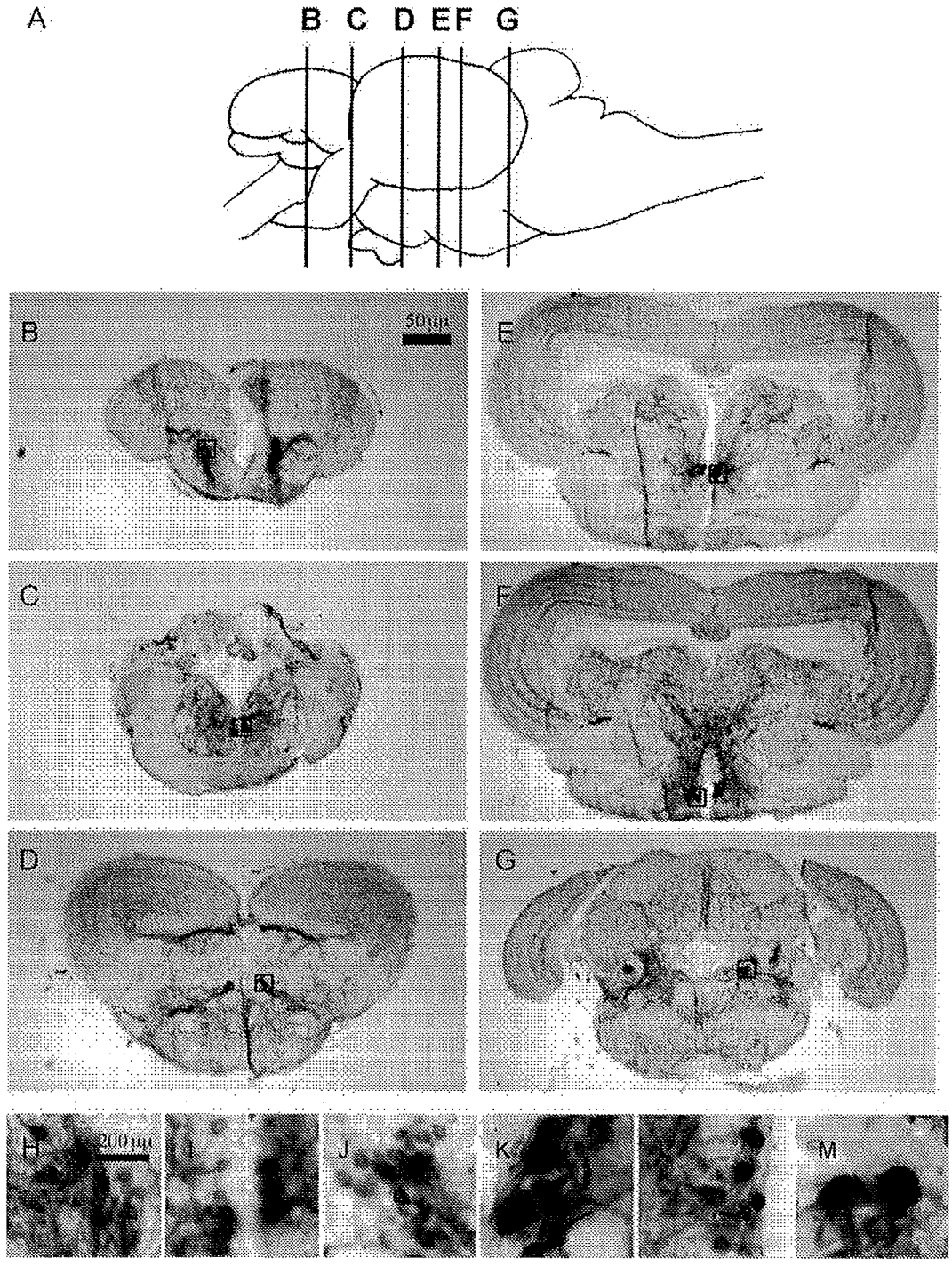

Fig. 1. The distribution of TH$^+$ neurons in adult medaka diencephalon and medulla oblongata. Coronal sections at different rostro-caudal levels show the localization of TH$^+$ dopaminergic fibers and neurons in the telencephalon (B), preoptic area (C) and diencephalon (D: rostral, E: middle, F: caudal). TH$^+$ neurons were also distributed in the medulla oblongata (G). Insets (H–M) are the magnified picture of original images (B–G) respectively. The positions of each section are illustrated by vertical lines in (A).

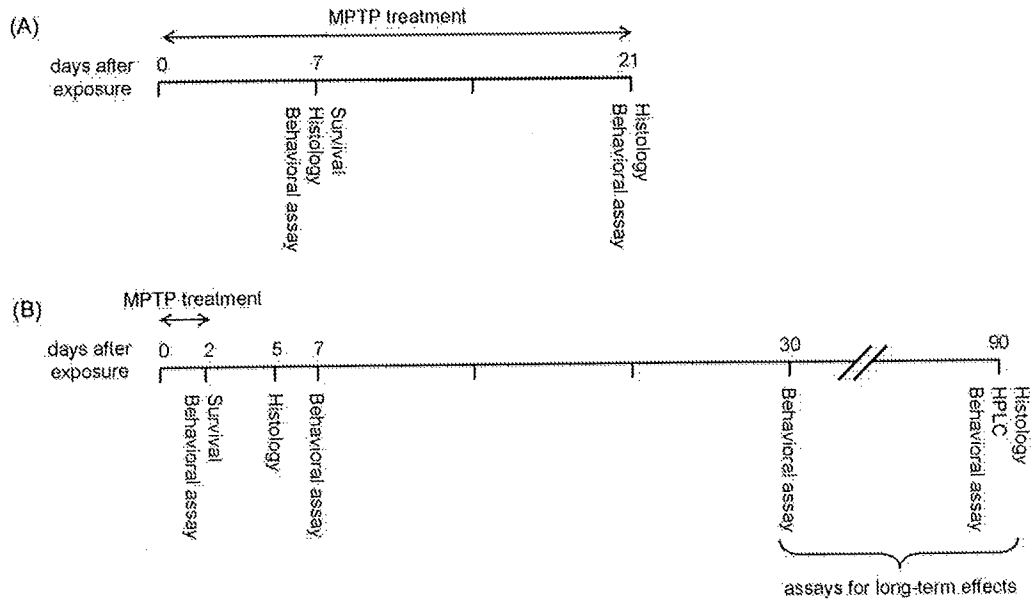

Fig. 2. MPTP treatment schedule. (A) For 3 weeks exposure to adult fish. 90-dpf fish were exposed to MPTP. MPTP was removed 21 days after the first exposure (111-dpf) and the brains of these fish were immediately fixed for histology. (B) For 2 days exposure to larvae. 10-dpf fish were exposed to MPTP. MPTP was removed 2 days after the first exposure (12-dpf). Assays including HPLC, behavioral analysis and histology were done at the indicated time course. The numbers indicate the days after the first exposure to MPTP.

(43.8 ± 4.2) in the medulla oblongata to monitor the effect of MPTP on noradrenergic neurons. In summary, we identified several clusters of TH^+ neurons in medaka brain and established a reliable method for evaluating the number of dopaminergic neurons.

3.2. Short-term effect of MPTP on adult and larval medaka

Several studies have been reported regarding the cytotoxic effect of MPTP on zebrafish and goldfish. In order to investigate the interspecies differences of sensitivity to MPTP between medaka and other model teleost fish, we treated 3 months old and 10-dpf (days post-fertilization) medaka with varying concentration of MPTP for 1 week (Fig. 2A). The embryonic development is slow in medaka in comparison to zebrafish, and it usually takes 7–10 days for medaka larvae before hatching out of the eggshell.

When the adult fish were exposed to 0.1 μg/ml of MPTP, all the fish (10 out of 10) survived a-week-long treatment, whereas 0.2 μg/ml of MPTP was tolerated by only a small fraction of fish (2

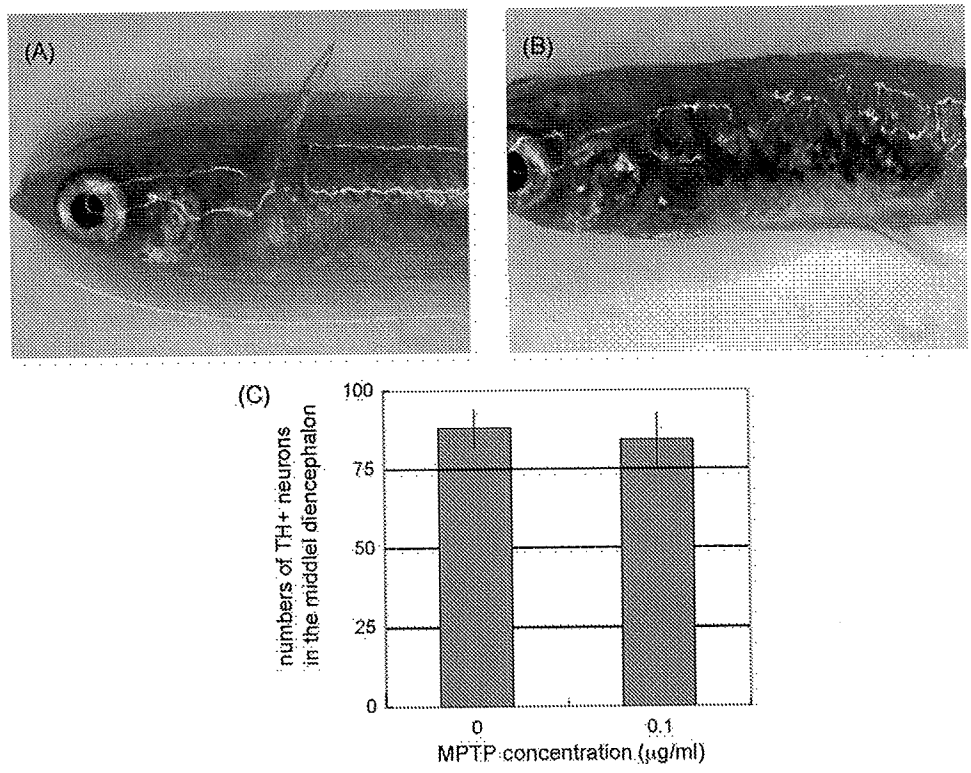

Fig. 3. Features of fish exposed to MPTP at the adult stage. (A and B) Skin images of control fish (A) and MPTP-treated fish (B). The skin was darkened by MPTP treatment (white allow). (C) The numbers of TH^+ neurons in the middle diencephalon. There was no significant reduction in the TH^+ neurons of MPTP-treated fish. $n = 8$ for each group.